Quantum partition functions from classical distributions: Application to rare-gas clusters

F. Calvo,[a] J. P. K. Doye, and D. J. Wales
University Chemical Laboratory, Lensfield Road, Cambridge CB2 1EW, United Kingdom

(Received 5 December 2000; accepted 8 February 2001)

We investigate the thermodynamic behavior of quantum many-body systems using several methods based on classical calculations. These approaches are compared for the melting of Lennard-Jones (LJ) clusters, where path-integral Monte Carlo (PIMC) results are also available. First, we examine two quasiclassical approaches where the classical potential is replaced by effective potentials accounting for quantum corrections of low order in $\hbar$. Of the Wigner–Kirkwood and Feynman–Hibbs effective potentials, only the latter is found to be in quantitative agreement with quantum simulations. However, both potentials fail to describe even qualitatively the low-temperature regime, where quantum effects are strong. Our second approach is based on the harmonic superposition approximation, but with explicit quantum oscillators. In its basic form, this approach is in good qualitative agreement with PIMC results, and becomes more accurate at low temperatures. By including anharmonic corrections in the form of temperature-dependent frequency shifts, the agreement between the quantum superposition and the PIMC results becomes quantitative for the caloric curve of neon clusters. The superposition method is then applied to larger clusters to study the influence of quantum delocalization on the melting and premelting of LJ_{19}, LJ_{31}, LJ_{38}, and LJ_{55}. The quantum character strongly affects the thermodynamics via changes in the ground state structure due to increasing zero-point energies. Finally, we focus on the lowest temperature range, and we estimate the Debye temperatures of argon clusters and their size variation. A strong sensitivity to the cluster structure is found, especially when many surface atoms reorganize as in the anti-Mackay/Mackay transition. In the large size regime, the Debye temperature smoothly rises to its bulk limit, but still depends slightly on the growth sequence considered. © *2001 American Institute of Physics.* [DOI: 10.1063/1.1359768]

I. INTRODUCTION

Classical many-body systems in thermal equilibrium are commonly investigated by means of computer simulations such as Monte Carlo (MC) or molecular dynamics (MD).[1] These methods in principle provide ''exact'' results for arbitrarily complex intermolecular forces, their only limitation being computational power. Quantum systems can also be studied by numerical simulation, and the most rigorous approaches at finite temperature are based on the path-integral treatment of quantum mechanics. Path-integral Monte Carlo (PIMC) methods have proven extremely useful and successful in predicting the thermodynamics properties of many condensed matter systems,[2,3] and, more recently, of finite atomic[4–7] and molecular[8] clusters. Two kinds of PIMC methods are in use, namely the Fourier-path-integral (FPI) (Ref. 9) and the discretized-path-integral (DPI) (Ref. 10) methods. They differ in how the paths are represented, but have been shown to yield essentially similar results.[11]

Although PIMC simulations incorporate quantum delocalization, they still contain approximations at the computational level. In both FPI and DPI methods, the path integrals are represented by a finite set of parameters (respectively, Fourier or Lie–Trotter coefficients), instead of the infinite number required for the methods to be rigorously exact. Practically, the number of parameters can be kept moderately small for systems that are neither too cold nor too delocalized. However, because of this limitation, the calculation of accurate thermodynamic properties, such as the caloric curve or the heat capacity, is hindered by the slower convergence of PIMC-type simulations at very low temperatures. In addition, the extra degrees of freedom arising in path-integral calculations act as replicas of the system, hence multiplying the effective computational complexity.

This problem can be at least partially handled for quasiclassical systems using effective potentials. These potentials may be viewed as expansions in $\hbar$ of the quantum partition function, either in the path-integral formalism,[12] or in the semiclassical Wigner–Kirkwood approach.[13] They provide a powerful technique for obtaining quantum corrections to mostly classical systems, without requiring full path-integral calculations. In particular, for atomic and molecular liquids, they have given very satisfactory results.[10,14–16] On the other hand, solids displaying a non-negligible quantum character are not well described by such potentials.[15] In this case, further refinements of the path-integral theory have been proposed[17] to formulate effective potentials valid even in the zero temperature limit. In particular, a quite efficient and elegant approach is that of Voth and co-workers,[18,19] based

[a]Permanent address: Laboratoire de Physique Quantique, IRSAMC, Université Paul Sabatier, 118 Route de Narbonne, F31062 Toulouse Cedex, France. Electronic mail: florent@irsamc.ups-tlse.fr

 © 2001 American Institute of Physics

Downloaded 25 May 2001 to 131.111.112.18. Redistribution subject to AIP license or copyright, see http://ojps.aip.org/jcpo/jcpcr.jsp

on self-consistent harmonic oscillators. The idea is to replace the actual quantal and anharmonic system near an equilibrium configuration by a set of equivalent oscillators.[18] This approach is also useful in studying the dynamics of the system, and has recently been applied to the classical and quantum theories of solvation in glassy systems.[19] However, all these self-consistent potentials must be recalculated at each new temperature and for each configuration, which make them very demanding from a computational point of view.

Another approach to compute the thermodynamic properties of a complex many-body system consists of summing the contributions of all basins of attraction of the configuration space, the so-called inherent structures,[20] to the partition function. This approach was pioneered by Stillinger and Weber,[20] then formalized in cluster physics,[21,22] and more recently used in the physics of liquids and glasses.[23] In classical systems, it has proved very useful in elucidating the relationships between the thermodynamics of clusters and their energy landscapes.[24,25] Stillinger formally extended the idea of partitioning the configuration space to the case of quantum systems,[26] however, only a few applications were made due to the required use of path-integral calculations.[27,28] A related approach uses instantaneous normal mode (INM) analysis to probe the structural or thermodynamical changes in classical or quantum systems.[29] One goal of this article is to extend the superposition method to quantum systems. We have chosen to test our methods on atomic clusters for which path-integral Monte Carlo data is available.[5–7] We have also tried to investigate systems currently too complex for full quantum simulations because of quasiergodicity problems that slow down the convergence considerably at low temperature.

Following the results of Chakravarty,[6,7] we attempt to rationalize the effects of quantum delocalization on cluster melting. Traditionally, these effects are quantified by λ, the thermal de Broglie wavelength at temperature T, where $\lambda = \hbar/\sigma\sqrt{mk_BT}$, σ is the interatomic equilibrium distance, and m is the atomic mass. If we denote the depth of the potential well by ε, then the extent of quantum delocalization effects is measured by the de Boer parameter $\Lambda = \hbar/\sigma\sqrt{m\varepsilon}$. The quantum superposition method developed in the present paper allows us to investigate *continuous* ranges of Λ, instead of only a set of prescribed values. Thus it allows a more complete picture of how quantum effects influence cluster thermodynamics.

Another objective is to investigate the very low temperature regime in more detail, where only a few dynamical calculations are available apart from classical studies. We first estimate the contribution of the zero-point energy to the total energy for clusters containing up to 150 rare-gas atoms, as well as for some different growth sequences. In many cases, the global minimum geometry is seen to change when some very soft vibrational modes are present, even in the case of argon clusters that are usually considered as classical systems. In this low-temperature regime structural transitions may still be observed, but their thermodynamic signature is smeared out, and disappears for stronger quantum delocalization.

The specific case of clusters trapped in a single solidlike local minimum is also considered, and we estimate the Debye temperatures of argon clusters and their variation with size. A very strong, nonmonotonic dependence on the structure is found for the smaller sizes. In particular, we are able to relate the variations of the Debye temperatures to changes in the surface structure, in agreement with the trends observed for the zero-point energies. The Debye approximation itself needs to be critically examined for clusters, as it involves a complete neglect of the high-frequency part of the vibrational spectrum. By looking at two large clusters, with crystalline and amorphous structures, we hope to gain insight into how closely clusters of a few hundreds of atoms can approach the bulk limit.

The article is organized into six main sections and a conclusion. In Sec. II, we briefly review the effective potential approaches of quasiclassical theories, and their use in computer simulations. We then test two of them, namely the quadratic Feynman–Hibbs (FH) potential and the Wigner–Kirkwood (WK) potential in the Fujiwara–Osborn–Wilk representation, on the 13-atom Lennard-Jones (LJ) cluster at various degrees of quantum delocalization. We then consider in Sec. III the quantum two-state model in the harmonic approximation, and its quasiclassical FH expansion. This simple model serves as a basis for the quantum superposition method, and allows us to obtain a qualitative picture of the quantum effects on cluster melting. In Sec. IV we extend the harmonic superposition method to the quantum case, and we again test it on the LJ_{13} cluster. We also compare its predictions to the quasiclassical harmonic superposition for which the quadratic FH potential is exact. We include anharmonic corrections in the quantum superposition, and find that these corrections produce good quantitative agreement with PIMC results. In Sec. V we apply the method to larger clusters, where little data is available. Some of these clusters are a challenge to simulation, even classically, because of the multiple-funnel energy landscapes they exhibit.[30] We also introduce stability diagrams where the ''phase'' of the cluster can be obtained from a bidimensional plot in the (Λ, T) plane. In Sec. VI, we focus more specifically on the static properties such as the influence of zero-point energies on the stability of the global minima. We also study the very low temperature thermodynamic behavior and estimate the Debye temperature of argon clusters. Finally, we report our conclusions in Sec. VII.

II. QUASICLASSICAL APPROACHES

Effective potentials have long been used in condensed matter physics as a cheap way of incorporating quantum corrections to classical properties. In cluster physics, they have been employed by Chakravarty to study isotopically mixed clusters.[31] It is well known that their reliability is mainly dependent on how far the system is from classical behavior, and also on the number of correction terms included in the expansion.

In this work we have considered two such low-order effective potentials that have been previously used in simulations of bulk systems.[15,16,32] By expanding the path-integral partition function around the classical path, Feynman and

Downloaded 25 May 2001 to 131.111.112.18. Redistribution subject to AIP license or copyright, see http://ojps.aip.org/jcpo/jcpcr.jsp

Hibbs have shown that the following Gaussian effective potential provides an approximation to the quantum free energy:[12]

$$V_{\mathrm{GFH}}(\mathbf{R},\beta)=\left(\frac{6m}{\pi\beta\hbar^2}\right)^{\kappa} 2\int V(\mathbf{R}+\mathbf{R}') \times\exp(-6m\mathbf{R}'^2/\beta\hbar^2)d\mathbf{R}'. \quad (1)$$

In this equation, $V(\mathbf{R})$ is the classical potential function of the $\kappa=3N-6$ atomic coordinates $\mathbf{R}=\{\mathbf{R}_i\}$, m is the atomic mass, and $\beta=1/k_BT$. In general, the Gaussian Feynman–Hibbs potential can be calculated analytically only for potentials V that can be written as a sum of Gaussian functions. This effective representation then becomes very system-dependent, and we give in Appendix A a way of obtaining it for the Lennard-Jones potential.

For a general (non-Gaussian) pairwise potential $V(\mathbf{R})=\Sigma_{i<j}v(r_{ij})$, it is also possible to expand the Gaussian Feynman–Hibbs potential into an effective pairwise potential $v_{\mathrm{FH}}(r_{ij})$, which is simply

$$v_{\mathrm{FH}}(r_{ij},\beta)=v(r_{ij})+\frac{\beta\hbar^2}{24m}\nabla^2 v(r_{ij}), \quad (2)$$

to first order in $\hbar^2$, where ∇^2 is the Laplacian operator.

Another way to construct effective potentials is based on the semiclassical Wigner–Kirkwood expansion.[13] To first order in $\hbar^2$, it yields

$$V_{\mathrm{WK}}(\mathbf{R},\beta) =V(\mathbf{R})-\beta^{-1}\ln\left[1-\frac{\beta^2\hbar^2}{12m}\sum_{i<j}\left(\nabla_i^2V_{ij}-\frac{\beta}{2}(\nabla_iV_{ij})^2 +\frac{\beta}{2}\nabla_iV_{ij}\cdot\sum_{k\neq i,j}\nabla_k(V_{ki}-V_{kj})\right)\right], \quad (3)$$

with ∇_i the gradient vector with respect to the coordinates of atom i. Following the resummation method of Fujiwara, Osborn, and Wilk,[33] Neumann and Zoppi[15] have developed effective pairwise potentials based on the WK expansion. Neglecting the three-body term in Eq. (3), we get the density-independent pair potential[15]

$$v_{\mathrm{WK}}(r_{ij},\beta)=v(r_{ij})+\frac{\beta\hbar^2}{12m}\nabla^2v(r_{ij})-\frac{\beta^2\hbar^2}{24m}[\nabla v(r_{ij})]^2. \quad (4)$$

The Wigner–Kirkwood expansion thus involves more terms, making the computation of the effective potential more demanding. Furthermore, as noted by Neumann and Zoppi,[15] the last term in v_{WK} is proportional both to β^2 and to the square of the force ∇v, and is also *attractive*. Hence, low temperatures will favor the collapse of all particles, a highly undesirable situation. To solve this problem requires one either to incorporate higher-order terms in the semiclassical expansion, or to introduce an artificial short-range cut-off in the potential preventing the collapse. However, the common problem of such expansions, including the Feynman–Hibbs expansion, is that higher order terms in $\hbar^2$ are also of higher order in β. Consequently, the low-temperature behavior will necessarily be unphysical at this level of theory.

With the above problems in mind, we have tested these two effective pairwise potentials on a system where more accurate results have been previously obtained, namely, the 13-atom Lennard-Jones cluster. The quasiclassical simulations were performed by parallel tempering Monte Carlo (PTMC),[34] using 50 temperatures regularly spaced in the range $0.01\leqslant T\leqslant 0.50$, and 10^5 MC sweeps for each temperature following 2×10^4 thermalization sweeps. Parallel tempering exchanges were attempted with 10% probability. All results are given in reduced LJ units of mass m, energy ε, and length σ. The extent of quantum delocalization is given entirely by the de Boer parameter Λ, which corresponds to the value of the constant $\hbar$ in the LJ reduced units system. The following cases have been investigated: LJ_{13} (classical, $\Lambda=0$), Xe_{13} ($\Lambda=0.01$), Ar_{13} ($\Lambda=0.03$), and Ne_{13} ($\Lambda=0.095$). For this latter cluster, we can compare our results to the accurate data recently obtained by Neirotti, Freeman, and Doll (NFD).[5] A cut-off radius of $r_{\mathrm{cut}}=1.06\sigma$ was necessary for Ne_{13} in order to obtain physically meaningful results in this range of temperatures for the WK potential. For all simulations, we enclosed the cluster inside a hard-wall sphere to prevent evaporation. The radius was chosen to be 2.5σ with respect to the cluster center of mass.

The heat capacities of the four clusters described by the two effective quasiclassical potentials are shown in Fig. 1. They were obtained from the partition function Z by the usual formula $C_v(\beta)=k_B\beta^2\partial^2\log Z/\partial\beta^2$, which can be written in terms of the following averages for a temperature-dependent potential $V_{\mathrm{eff}}(\beta)$:

$$C_v(\beta)=k_B\beta^2\left[\left\langle\left(\frac{\partial\beta V_{\mathrm{eff}}}{\partial\beta}\right)^2\right\rangle-\left\langle\frac{\partial\beta V_{\mathrm{eff}}}{\partial\beta}\right\rangle^2-\left\langle\frac{\partial^2\beta V_{\mathrm{eff}}}{\partial\beta^2}\right\rangle\right]. \quad (5)$$

Incidentally, this equation shows that negative heat capacities are possible if the effective potential grows with β, as it does in the Feynman–Hibbs approximations. We find in Fig. 1 that both the FH and WK potentials fail at low temperatures, as expected from previous studies.[15,32] The use of a Gaussian-expanded LJ potential and the Gaussian–Feynman–Hibbs effective potential does not help to solve this problem.

The caloric curves calculated with the FH potential show a decrease in the heat capacity peak as well as a decrease in the melting point as Λ increases. The effect is already perceptible for xenon, and reaches about 10% for neon with respect to the classical behavior. The heat capacity peak decreases from about $110k_B$ to about $70k_B$ for Ne_{13}, which together with the variations in the melting point, are in very good agreement with PIMC results.[5,6] Above the melting point, the curves we find are slightly different from Neirotti and co-workers' results, but we believe the differences result from the different constraining potentials. Below the melting point, the same comparison shows that the FH potential ceases to be valid near $T\sim0.2\,\varepsilon/k_B$ for neon.

The situation is quite different for the Wigner–Kirkwood potential.[2] Because of the large cut-off used to truncate the repulsive part of the LJ potential, the caloric curves are affected throughout the temperature range, and differ from the classical behavior (with the untruncated LJ

Downloaded 25 May 2001 to 131.111.112.18. Redistribution subject to AIP license or copyright, see http://ojps.aip.org/jcpo/jcpcr.jsp

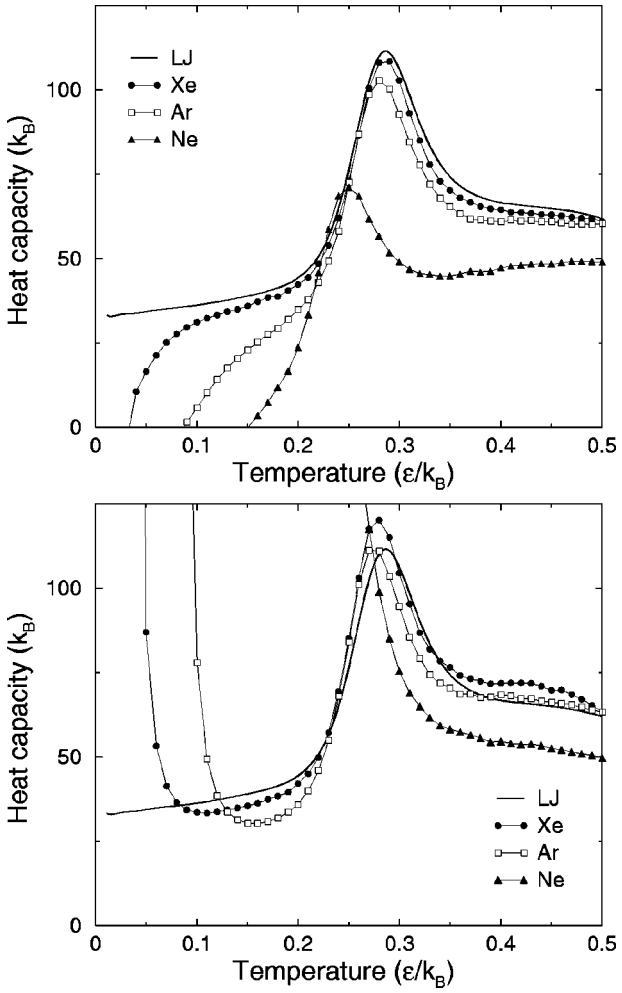

FIG. 1. Heat capacities of LJ_{13} clusters at various degrees of quantum delocalization, calculated from Monte Carlo simulations using effective classical potentials. Results are shown for the classical case ($\Lambda=0$), for xenon ($\Lambda=0.01$), argon ($\Lambda=0.03$), and neon ($\Lambda=0.095$). Upper panel: calculations with the Feynman–Hibbs potential; lower panel: calculations with the Wigner–Kirkwood potential.

potential) even at high temperatures. For xenon and argon, the lower limit of validity of the quasiclassical WK approximation is similar to the FH lower limit, near $0.1\,\varepsilon/k_B$ and $0.16\,\varepsilon/k_B$, respectively. Below these values, the potential and internal energies drop causing the heat capacity to rise sharply as T goes to zero. The variations of the caloric curves in the nearly classical regime are close to those obtained with the FH potential. For Ne_{13} we have not been able to obtain reliable results below the classical melting temperature. Increasing the cut-off radius beyond 1.06σ leads to very unphysical potentials behaving significantly differently from the original LJ potential. We have tried to improve this situation by adding the three-body terms of Eq. (3), but the effect on the caloric curves is small.

Thus, at the lowest order in quantum corrections, only the Feynman–Hibbs effective potential seems able to account for the quasiclassical thermodynamic behavior of rare-gas clusters as light as Ne_{13}. In contrast, the Wigner–Kirkwood potential has trouble properly describing the solidlike phase, which makes it unsuitable for investigating melting in clusters exhibiting a noticeable quantum character. However, even the FH approximation will fail at higher and higher temperatures, as quantum delocalization increases beyond that observed in neon. Moreover, the present effective potentials are not able to account for all the possible low-temperature effects characteristic of clusters, such as isomerization and premelting.[35] These results lead us to look for alternative treatments that are valid at very low temperatures, and retain the physical features of the various phase-like forms of clusters.

III. TWO-STATE QUANTUM MODEL AND THE QUASICLASSICAL REGIME

Although only qualitative, the two-state model[36] has proved useful in analyzing the dynamical coexistence reported in the 1980s by Berry and co-workers.[37] Basically, the model consists of assuming that the system can access only two states, respectively solidlike and liquidlike, characterized by ground state energies E_S and E_L, vibrational (normal mode) frequencies ν_S^i and ν_L^i, $i=1,\ldots,\kappa=3N-6$, and degeneracies n_S and n_L. The partition function of the system is then simply the sum of the two individual partition functions $Z(T)=Z_S(T)+Z_L(T)$, and all thermodynamic properties follow from this definition.

The harmonic approximation for each partition function is sufficient to show that the system undergoes a ''phase change'' between the state of lowest energy (S) and the other state (L) at a temperature where the internal energy rises and the heat capacity reaches its maximum. Of course, this transition can be very gradual and depends on the size as well as the ratios of the vibrational frequencies and degeneracies. To go beyond the classical picture and include quantum effects, we consider the partition functions Z_S and Z_L in their fully quantum forms, where Z can be written as

$$Z^{\mathrm{Q}}(\beta)=n_S\exp(-\beta E_S)\prod_{i=1}^{\kappa}\frac{e^{-\beta h\nu_S^i/2}}{1-e^{-\beta h\nu_S^i}} + n_L\exp(-\beta E_L)\prod_{i=1}^{\kappa}\frac{e^{-\beta h\nu_L^i/2}}{1-e^{-\beta h\nu_L^i}}. \quad (6)$$

Such an approach has been used by Franke and co-workers[22] to study isomerization between the two states of LJ_6. In Eq. (6), we have made the approximation that the wave functions inside each basin do not interfere. Of course, for $h\to 0$ we recover the usual classical expression $Z^{\mathrm{C}}(\beta)=n_S e^{-\beta E_S}/(\beta h\overline{\nu_S})^{\kappa}+n_L e^{-\beta E_L}/(\beta h\overline{\nu_L})^{\kappa}$, where $\overline{\nu}$ is the geometric mean value of the ν^i's. If the temperature is not too low, it is also possible to use a quasiclassical expansion of the classical partition function, by noting that the quadratic Feynman–Hibbs expansion becomes exact for harmonic oscillators.[12] In this case, we just have to replace the energies E_α by their effective values $E_\alpha^{\mathrm{FH}}(\beta)$, with $\alpha=S$ or L,

$$E_\alpha^{\mathrm{FH}}(\beta)=E_\alpha+\frac{\beta h^2}{24}\sum_i(\nu_\alpha^i)^2=E_\alpha+\kappa\frac{\beta h^2}{24}(\nu_\alpha^{\mathrm{rms}})^2, \quad (7)$$

Downloaded 25 May 2001 to 131.111.112.18. Redistribution subject to AIP license or copyright, see http://ojps.aip.org/jcpo/jcpcr.jsp

with the root mean square vibrational frequencies $\nu_\alpha^{\mathrm{rms}}$. By performing a simple semiclassical expansion of the quantum partition function,

$$\prod_{i=1}^{\kappa} \frac{e^{-\beta h \nu^i/2}}{1-e^{-\beta h \nu^i}} = \frac{1}{(\beta h \overline{\nu})^\kappa}\left[1-\kappa\frac{\beta^2 h^2}{24}(\nu^{\mathrm{rms}})^2+O(h^4)\right], \quad (8)$$

we recover the Feynman–Hibbs expansion of the effective energies. The low-temperature behavior in the quasiclassical approximation is unphysical, which is hopefully not the case in the quantum model. To see what qualitative differences are introduced by the quantum character of the oscillators, we introduce the arithmetic average of the vibrational frequencies, $\langle \nu_\alpha \rangle = (\Sigma_i \nu_\alpha^i)/\kappa$, and we write Eq. (6) as

$$Z^{\mathrm{Q}}(\beta) = n_S \frac{e^{-\beta E_S^0}}{\Pi_i 1-e^{-\beta h \nu_S^i}}\left[1+\frac{n_L}{n_S}e^{\beta(E_S^0-E_L^0)}\prod_i \frac{1-e^{-\beta h \nu_S^i}}{1-e^{-\beta h \nu_L^i}}\right], \quad (9)$$

where $E_\alpha^0 = E_\alpha + \kappa h \langle \nu_\alpha \rangle/2$ is the ground state energy including the zero-point energy. The most stable state is found by looking at which term dominates Z^{Q} at a given temperature. In particular, the zero temperature limit gives

$$Z^{\mathrm{Q}}(\beta \to \infty) \sim n_S e^{-\beta E_S^0} + n_L e^{-\beta E_L^0}. \quad (10)$$

Therefore the effective ground state is the one with the lowest E^0. A problem could appear if $\langle \nu_L \rangle < \langle \nu_S \rangle$ and if quantum delocalization is high enough to exchange the relative stabilities of the S and L states, as the latter would never be populated.

We have been unable to extract exact analytic results for the influence of quantum effects on the heat capacity maximum. Instead, we simplify the problem by assuming that melting occurs when the two states become equally probable: $Z_S(T=T_{\mathrm{melt}}) = Z_L$. Then the melting point $T_{\mathrm{melt}} = 1/k_B\beta$ satisfies

$$e^{\beta(E_L^0-E_S^0)} = \frac{n_L}{n_S}\prod_i \frac{1-e^{-\beta h \nu_S^i}}{1-e^{-\beta h \nu_L^i}}. \quad (11)$$

In the quasiclassical (QC) regime, a Taylor expansion can be performed, and we obtain the relative variations of T_{melt} with increasing h as

$$T_{\mathrm{melt}}^{\mathrm{QC}}(h) = T_0\left[1-\frac{\kappa h^2}{24 T_0 \Delta E}(\nu_S^{\mathrm{rms}}-\nu_L^{\mathrm{rms}})(\nu_S^{\mathrm{rms}}+\nu_L^{\mathrm{rms}}) + O(h^4)\right], \quad (12)$$

where $\Delta E = E_L - E_S$, and where $T_0 = T_{\mathrm{melt}}(0)$ is the classical melting temperature given by $T_0 = \Delta E/\Gamma$ with

$$\Gamma = \ln\left[\frac{n_L}{n_S}\left(\frac{\overline{\nu_S}}{\overline{\nu_L}}\right)^\kappa\right]. \quad (13)$$

The same result is obtained by considering the semiclassical superposition for a small value of h. However, in the Feynman–Hibbs approximation, the exact calculation of T_{melt} at any value of h (less than a maximum value, see below) is possible, and the result is simply

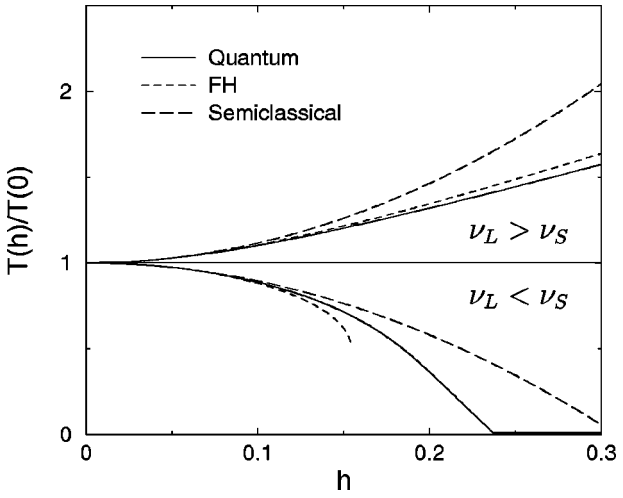

FIG. 2. Variations of the melting temperature in the two-state harmonic model induced by quantum delocalization. The results are plotted for two values of the vibrational frequency of the liquid state, respectively, smaller and greater than the solid state frequency, and for the full quantum model, the Feynman–Hibbs approximation, and the first-order semiclassical expansion.

$$T_{\mathrm{melt}}^{\mathrm{FH}}(h) = \frac{T_0}{2}\left[1+\left(1-\frac{\kappa h^2}{6 T_0 \Delta E}(\nu_S^{\mathrm{rms}}-\nu_L^{\mathrm{rms}}) \times (\nu_S^{\mathrm{rms}}+\nu_L^{\mathrm{rms}})\right)^{1/2}\right]. \quad (14)$$

Equations (12) and (14) show that the variations in the melting point depend essentially on the relative values of the mean square vibrational frequencies. The usual situation for clusters is that ν_S and ν_L are comparable, ν_S being somewhat larger than ν_L especially for very symmetric geometries. Hence we can expect a decrease in T_{melt}, which will be larger for high symmetry ''magic number'' clusters provided that the effect of the larger ν_S^2 is larger than that of the larger ΔE.

We have plotted in Fig. 2 the variations of the melting point as a function of quantum delocalization for the two cases $\nu_S^{\mathrm{rms}} < \nu_L^{\mathrm{rms}}$ and $\nu_S^{\mathrm{rms}} > \nu_L^{\mathrm{rms}}$. For simplicity, all frequencies were given the same value for each state S or L: $\nu_\alpha^i = \nu_\alpha^{\mathrm{rms}} = \overline{\nu_\alpha} = \langle \nu_\alpha \rangle$. T_{melt} was calculated by equating Z_S and Z_L, and two cases were studied, with $\nu_S = 1$, $\nu_L = 0.9$, and $\nu_L = 1.1$, respectively, for a 30-atom system with $\Delta E = 1$. n_S/n_L was adjusted to keep the classical melting point at a constant value. In Fig. 2 we have compared the value in the quantum model to the FH approximation and to the simple expansion (12). The quasiclassical Feynman–Hibbs approximation is quite accurate when $\nu_L > \nu_S$, but fails completely as soon as $h > h_{\max} = (6 T_0 \Delta E/\kappa(\nu_S^2 - \nu_L^2))^{1/2} \simeq 0.15$, when $\nu_L < \nu_S$. Again, this shows that quasiclassical effective potentials should be used with caution when dealing with strong quantum effects.

IV. QUANTUM HARMONIC SUPERPOSITION APPROXIMATION

The two-state model of the previous section is a very simplified representation of a many-body system with a mul-

Downloaded 25 May 2001 to 131.111.112.18. Redistribution subject to AIP license or copyright, see http://ojps.aip.org/jcpo/jcpcr.jsp

tidimensional energy landscape. However, it contains the fertile concept of relating the global thermodynamic properties to local features of these landscapes, namely, the energies and vibrational frequencies of local minima. Such an approach has been considered before,[38] but the lack of powerful computational tools for exploring energy landscapes hindered its fruitful development until the last decade. With the notion of inherent structures introduced by Stillinger and Weber in bulk studies,[20] came the idea of dividing the configuration space into basins of attraction, and building the partition function as the sum of all contributions from each basin. The problem then becomes the calculation of these individual partition functions, whose number grows exponentially with the system size.

Various studies by Wales, Doye, and others[21,24,25,39] have demonstrated how this superposition method can be implemented in practice for clusters in the classical regime, at various levels of approximation.[40,41] Here the main motivation has been to show in detail how the thermodynamic properties emerge from the characteristics of the energy landscape. In the simplest version of the superposition method, each local minimum α is treated as a collection of κ uncoupled harmonic oscillators of frequencies ν_α^i, $i=1,\ldots,\kappa$. Thus the classical partition function for one particular minimum is written[21]

$$Z_\alpha(\beta)=\frac{e^{-\beta E_\alpha}}{(\beta h\bar{\nu}_\alpha)^\kappa}=Z_\alpha^C(\beta), \tag{15}$$

where the superscript C stands for classical. The total partition function for the whole set of minima is

$$Z(\beta)=\sum_\alpha n_\alpha Z_\alpha(\beta), \tag{16}$$

where the sum is over all geometrically distinct minima on the potential energy surface, with n_α the number of permutational isomers of minimum α. If the system is made of N identical atoms, n_α is given by $n_\alpha=2N!/h_\alpha$, h_α being the order of point group of structure α.

A. Superposition of quantum oscillators

Following the approach of Sec. III, we attempt to include quantum effects in the thermodynamic properties by simply replacing the classical oscillators with quantum ones,

$$Z_\alpha(\beta)=e^{-\beta E_\alpha}\prod_{i=1}^{\kappa}\frac{e^{-\beta h\nu_\alpha^i/2}}{1-e^{-\beta h\nu_\alpha^i}}=Z_\alpha^{\mathrm{Q}}(\beta). \tag{17}$$

In the classical limit, one of the major approximations of the harmonic superposition method is that it neglects the overlapping of the individual contributions to Z. This approximation remains in the case of quantum oscillators, but Eq. (17) assumes in addition that no quantum interference occurs to modify the energy levels of local minima, i.e., the present quantum superposition assumes there is no tunneling.

Practically, Eq. (17) together with Eq. (16) are of little use if the set of minima in our database is far from complete, which is likely even for a few tens of atoms. To tackle this problem one can use the reweighting technique previously employed in the classical case,[21] which uses the results of a classical simulation. More precisely, we perform a canonical (MC or MD) simulation at inverse temperature β_0, and record the probability $p_\alpha(\beta_0)$ of finding isomer α. We write the total classical partition function as a sum over all known minima, but weighted by factors g_α to correct for the incompleteness of the set of minima,

$$Z^{\mathrm{C}}(\beta)\propto\sum_\alpha g_\alpha n_\alpha Z_\alpha^{\mathrm{C}}(\beta). \tag{18}$$

From the simulation, the number of quenches leading to isomer α is proportional to $p_\alpha(\beta_0)$, and also to $g_\alpha n_\alpha Z_\alpha^{\mathrm{C}}(\beta_0)$. This proportionality requires the simulation to be ergodic. The classical partition function for the incomplete sample is then approximated by

$$Z^{\mathrm{C}}(\beta)\propto\sum_\alpha p_\alpha(\beta_0)\frac{Z_\alpha^{\mathrm{C}}(\beta)}{Z_\alpha^{\mathrm{C}}(\beta_0)}. \tag{19}$$

Now we follow a similar procedure for the quantum case, except that we do not wish to perform a quantum simulation to obtain the weights. Actually, the weights should depend only on the topography of the energy surface, and not on the ensemble (microcanonical or canonical) or on the probability law used to generate the ensemble, quantum or classical, because they are related to the number of minima on the potential energy surface. In the case of a bulk system, these weights should also depend on the density or the pressure. The g_α's are the ratios of $p_\alpha(\beta_0)$ and $n_\alpha Z_\alpha(\beta_0)$, where Z_α is assumed to have been used to generate p_α. Thus we can employ the probabilities found in a classical simulation to estimate the weights g_α, which depend only on α, and in turn calculate the full quantum partition function as

$$Z^{\mathrm{Q}}(\beta)\propto\sum_\alpha p_\alpha(\beta_0)\frac{Z_\alpha^{\mathrm{Q}}(\beta)}{Z_\alpha^{\mathrm{C}}(\beta_0)}. \tag{20}$$

For large classical systems, the use of reweighted formulas such as Eq. (19) was shown to improve considerably the predictions of the harmonic superposition method,[21] in particular by reproducing the van der Waals loop in the microcanonical caloric curve of LJ_{55}.

We first tested the quantum superposition method on a cluster where our database of minima is almost complete, namely, LJ_{13}. From expressions (16) and (17) for the partition function, we calculated the heat capacity $C_v(\beta)$ from

$$C_v(\beta)=k_B\beta^2\left[\frac{Z_2+2Z_{11}+Z_{02}}{Z_0}-\left(\frac{Z_1+Z_{01}}{Z_0}\right)^2\right], \tag{21}$$

with the following terms ($Z_0=Z$):

$$Z_n=\sum_\alpha\frac{n_\alpha(E_\alpha^0)^n e^{-\beta E_\alpha^0}}{\Pi_i 1-e^{-\beta h\nu_\alpha^i}},\quad n=0,1,2, \tag{22}$$

$$Z_{n1}=\sum_\alpha\frac{n_\alpha(E_\alpha^0)^n e^{-\beta E_\alpha^0}}{\Pi_i 1-e^{-\beta h\nu_\alpha^i}}\sum_j\frac{h\nu_\alpha^j}{e^{\beta h\nu_\alpha^j}-1},\quad n=0,1, \tag{23}$$

Downloaded 25 May 2001 to 131.111.112.18. Redistribution subject to AIP license or copyright, see http://ojps.aip.org/jcpo/jcpcr.jsp

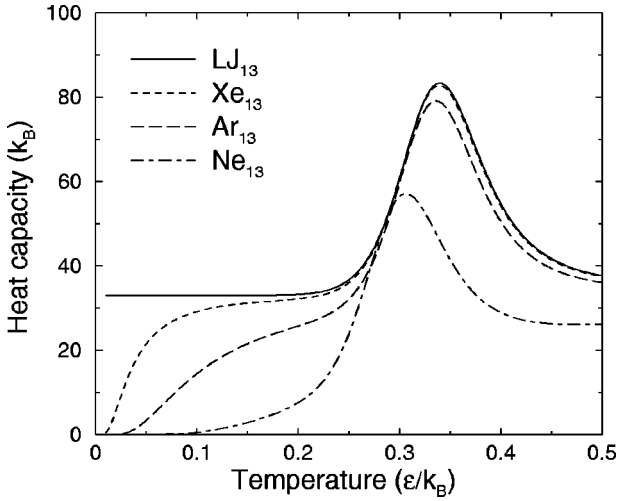

FIG. 3. Heat capacities of LJ_{13} from the quantum superposition method. The values of the de Boer parameter are the same as in Fig. 1.

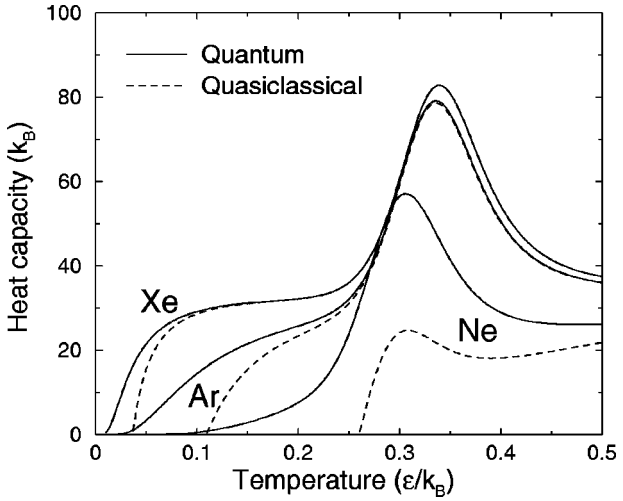

FIG. 4. Heat capacities of LJ_{13} from the quasiclassical superposition method. The values of the de Boer parameter are the same as in Fig. 1.

$$Z_{02}=\sum_{\alpha}\frac{n_{\alpha}e^{-\beta E_{\alpha}^{0}}}{\Pi_{i}1-e^{-\beta h\nu_{\alpha}^{i}}}\left[\sum_{j}\frac{(h\nu_{\alpha}^{j})^{2}e^{-\beta h\nu_{\alpha}^{j}}}{(1-e^{-\beta h\nu_{\alpha}^{j}})^{2}}+\left(\sum_{j}\frac{h\nu_{\alpha}^{j}}{e^{\beta h\nu_{\alpha}^{j}}-1}\right)^{2}\right], \tag{24}$$

and with the notation $E_{\alpha}^{0}=E_{\alpha}+\kappa h\langle\nu_{\alpha}\rangle/2$, where $\langle\nu_{\alpha}\rangle$ is the arithmetic average of the frequencies ν_{α}^{i}, $i=1,\ldots,\kappa$.

The results for four values of the quantum delocalization parameter and a sample of 1467 minima are shown in Fig. 3. The general picture is very similar to the quasiclassical results of Sec. II; the melting peak decreases with the atomic mass, and the melting temperature decreases up to about 10% for neon. The low temperature behavior is correct, at least qualitatively. This result was expected from the way that we constructed the partition function, and from the validity of the harmonic approximation at $T\rightarrow 0$. However, a precise comparison with the quasiclassical results or with the quantum MC results[5] reveals that the melting point is too high by about 15%, and that the peaks are too low also by 15%. As similar shifts are found for the classical harmonic superposition method,[21] the problem is not related to the choice of quantum oscillators, but rather to the approximation of harmonicity.

B. Quasiclassical superposition

By analogy to the way we have built the quantum partition function from individual quantum oscillators, we may consider the particular case of semiclassical oscillators where the energy of minimum α is replaced by its Feynman–Hibbs effective energy. Since we are dealing only with harmonic oscillators, this quasiclassical approximation is equivalent to expanding the quantum partition function to its lowest corrective order in h^2. Hence we write

$$Z_{\alpha}^{\mathrm{QC}}(\beta)=\frac{e^{-\beta E_{\alpha}}}{(\beta h\overline{\nu}_{\alpha})^{\kappa}}\left[1-\kappa\frac{\beta^{2}h^{2}}{24}(\nu_{\alpha}^{\mathrm{rms}})^{2}\right], \tag{25}$$

and the corresponding expressions for the total partition functions, with or without reweighting, follow from this equation. The heat capacity is given in Appendix B for this quasiclassical approximation. We have calculated the caloric curves for the same clusters as those studied in the quantum case, and the results are plotted in Fig. 4. Not surprisingly, we find good agreement with the quantum caloric curves down to limiting temperatures that increase with the degree of quantum delocalization. Below these temperatures, the quasiclassical approximation becomes unphysical ($C_v<0$). In the case of Ne_{13}, the caloric curve differs strongly from the quantum behavior, even if the quasiclassical curve exhibits the correct shift in the melting temperature. We also notice that the present quasiclassical approximation is in better agreement with the Gaussian Feynman–Hibbs effective potential (see Appendix A) than with the quadratic potential. Since the computational cost involved in quasiclassical calculations is only marginally lower than the cost of full quantum calculations, we have not considered the quasiclassical approach further. Instead, we have chosen to focus solely on the quantum superposition method.

As mentioned above, the agreement between the harmonic form of the quantum superposition and the PIMC results is not fully quantitative in the vicinity of the melting point. The problem was already noticed by Doye and Wales in the classical case,[40] and interpreted in terms of anharmonic effects. These effects were also seen to be more important for the 13-atom LJ cluster, where the basin of the icosahedral global minimum is very large, leading to some wide and flat regions in the energy landscape.[40] Doye and Wales managed to get agreement with simulations by incorporating these anharmonicity effects as corrections to the harmonic partition function. Here we will follow similar lines in an effort to improve the quantum superposition method.

C. Anharmonic corrections to the quantum partition function

In Ref. 40, Doye and Wales investigated two possible anharmonic contributions to the thermodynamic behavior,

Downloaded 25 May 2001 to 131.111.112.18. Redistribution subject to AIP license or copyright, see http://ojps.aip.org/jcpo/jcpcr.jsp

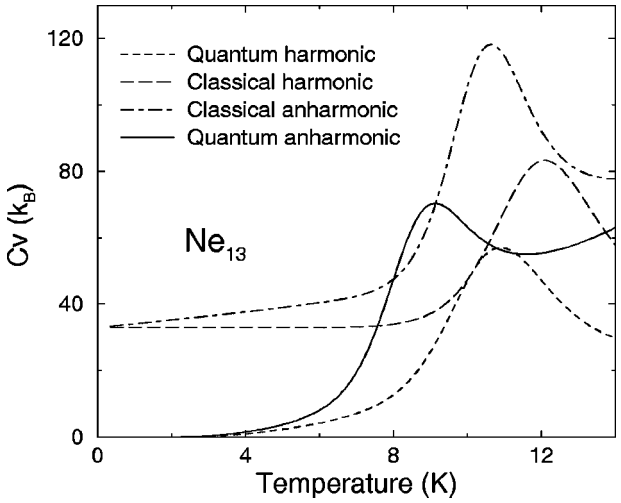

FIG. 5. Heat capacities of Ne_{13} in the classical and quantum regimes calculated from the quantum superposition method, with and without anharmonic corrections.

namely, the effects of transition state valleys and well anharmonicity. Their results suggest that the latter effects dominate, at least for the LJ clusters they investigated. In addition, we note that the transition state valleys could be accounted for in the same way as for the quantum oscillators by replacing the corresponding classical oscillators of Ref. 40 accordingly. More recently, Ball and Berry have also examined anharmonic corrections to the densities of states and found that the most appropriate form depended on the type of cluster.[41,42]

We first tried to correct for well anharmonicities using Morse oscillators instead of harmonic ones. This method was shown to work well as a correction for classical clusters,[40] however, a qualitative change occurs in the quantum regime due to the finite number of energy levels in a Morse oscillator, which caused large discrepancies in the final results.

Another way to incorporate well anharmonicities is phenomenological, and is often used in solid state physics.[43] It consists of allowing shifts in the vibrational frequencies induced by temperature changes. We have chosen to allow all frequencies ν_α^i to depend smoothly on temperature via the following simple expansion, to second order in T,

$$\nu_\alpha^i(T)=\nu_\alpha^i(0)[1-a_\alpha^i T-b_\alpha^i T^2]. \tag{26}$$

In the classical case, it is worth noting that the same expansion is obtained using Morse oscillators,[40] provided that b_α^i is set to $2(a_\alpha^i)^2$. To simplify the analysis, we have assumed that the a_α^i's and b_α^i's depend only on the geometry α but not on i. The expressions for the thermodynamic quantities become more complicated, and are given in Appendix C. We can now investigate the very low temperature behavior in the classical and quantum limits. The heat capacity is then found to behave as

$$C_v(\beta\to\infty)\sim\kappa k_B(1+2a/\beta) \text{ in the classical case,} \tag{27}$$

$$C_v(\beta\to\infty)\sim\kappa h\langle\nu(0)\rangle b k_B^3/\beta \text{ in the quantum case,} \tag{28}$$

and therefore has a linear component in both cases. As was observed by Doye and Wales,[40] it is difficult to estimate independently the correct values for the coefficients a_α and b_α. We propose to divide the set of isomers into several sets according to the topography of the energy landscape. In the case of LJ_{13}, the first set contains only the icosahedral minimum, and the second set contains all the remaining isomers. Then, by taking appropriate values for the coefficients a and b, we have obtained the caloric curves displayed in Fig. 5. In LJ units we took $a_{\rm I}=0.57$, $a_{\rm II}=0.67$, $b_{\rm I}=0.05$, and $b_{\rm II}=0.45$ for correcting both the classical and quantum caloric curves. The comparison with the results of Neirotti, Freeman, and Doll, is now much better: both the quantum and classical heat capacities have the correct widths, heights, and locations within the errorbars of the PIMC simulations.[5]

Hence, it appears that with only a few parameters, the above quantum superposition approach can be brought into quantitative agreement with path-integral Monte Carlo simulations. This method also allows us to study much larger systems, because it only requires information from classical calculations. The predicted effects of quantum delocalization on the melting of larger atomic van der Waals clusters are the subject of the next section.

V. LARGER SIZES AND STABILITY DIAGRAMS

We have selected four sizes in the range $13\leqslant N\leqslant 55$, which display several characteristics of cluster melting in classical simulations. The 19-atom cluster is particularly stable (''magic''), and has been previously investigated by Chakravarty using PIMC simulations.[6] Its solidlike–liquidlike phase change is very similar to that in LJ_{13}. The next magic cluster $N=55$ has a sharper melting peak, but is also similar to LJ_{13} in the classical regime.[44] We have also chosen two specific sizes that have more interesting size effects due to the peculiarities of their energy landscapes.[30]

The 31-atom Lennard-Jones cluster lies at the crossover between anti-Mackay (or polyicosahedral) geometries and Mackay (or multilayer icosahedral) geometries.[45] At this size, classical LJ_{31} is only slightly lower in energy in the Mackay structure. At very low temperatures, the cluster classically undergoes a structural transition between the two competing arrangements, and then, at much higher temperatures, is seen to melt by reaching a much larger set of minima.[46] The preliminary structural transition is sharp in this system, and leads to a very pronounced heat capacity peak.

The 38-atom cluster is now well known for its unusual truncated octahedral geometry.[47] The double-funnel energy landscape of this system[30,48] gives rise to a structural transition between the global minimum and the icosahedral minima with higher entropy.[24,49]

These two systems are difficult to study by standard simulation methods because of the structural transitions they exhibit. Classical simulations must be performed with special techniques to overcome the quasiergodic behavior, especially at low temperatures where interfunnel crossings are normally rare, if not forbidden in the microcanonical ensemble.[49] Even when using such techniques as parallel tempering (the most promising strategy at the present time), the convergence of thermodynamic averages is much slower for these clusters than for the single-funnel 19-atom and 55-

Downloaded 25 May 2001 to 131.111.112.18. Redistribution subject to AIP license or copyright, see http://ojps.aip.org/jcpo/jcpcr.jsp

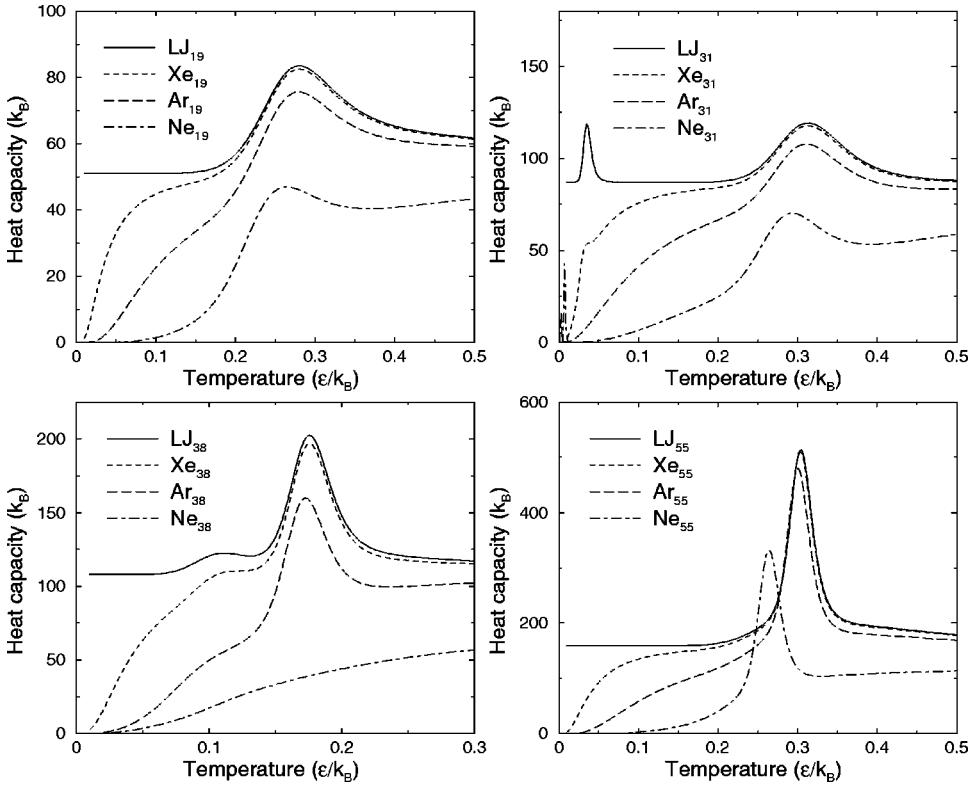

FIG. 6. Heat capacities of LJ_{19}, LJ_{31}, LJ_{38}, and LJ_{55} calculated from the quantum superposition method.

atom clusters, and involves up to 10^9 Monte Carlo cycles (and several tens of simultaneous simulations) for LJ_{38}. It is very likely that simulating LJ_{31} or LJ_{38} by quantum Monte Carlo methods at thermal equilibrium is not practical with the current computer technology. In these cases, the quantum superposition approach should be especially useful, since it is intrinsically ergodic once we have a representative sample of minima that includes the contributions of all important funnels. Nevertheless, application of this technique requires a reweighting of each individual partition function because an exhaustive sampling of the energy landscape is neither feasible, nor desirable.

We estimated all weights from classical MC simulations improved with parallel tempering in order to get better ergodic sampling. For LJ_{19} and LJ_{55}, the weights were calculated above the melting point, at $T=0.35\,\varepsilon/k_B$, and sets of 1259 and 3332 isomers were used, respectively. For LJ_{38}, the weights were calculated at a much lower temperature, $T=0.175\,\varepsilon/k_B$, where the global minimum, icosahedral minima, and liquidlike minima all have reasonably large probabilities of being visited.[24,48,49] 1881 different minima were recorded for this size. The case of LJ_{31} is a bit more problematic, because the probability of being in the global minimum basin was seen to drop nearly to zero at the Mackay/anti-Mackay transition temperature $T\sim 0.03\,\varepsilon/k_B$, while the liquidlike isomers start becoming populated only above $0.2\,\varepsilon/k_B$.[46] We have used the reweighting technique to calculate the relative weights of the liquidlike isomers with respect to one anti-Mackay minimum, and then added the contribution of the lowest-energy minimum,

$$Z(T)\simeq Z_{\text{lowest}}(T)+Z_{\text{others}}(T). \tag{29}$$

A similar approach has been used previously by Doye and Wales for the 38-atom cluster.[24] 2183 distinct minima were used for LJ_{31}, and the weights were calculated at $T=0.35\,\varepsilon/k_B$. After estimating the weights from classical simulations, we used them to compute the quantum partition functions following the method described in Sec. IV. We did not use anharmonic corrections in the four cases investigated here, because the agreement with classical simulations was already satisfactory, as far as the melting points are concerned. Moreover, such corrections would not give new insights into the effects of delocalization, so the present harmonic treatment is good enough for our purposes.

A. Caloric curves

The effects of quantum delocalization on the melting of LJ_{19}, LJ_{31}, LJ_{38}, and LJ_{55} can be seen in Fig. 6, where we represent the canonical heat capacities for values of Λ corresponding to classical behavior, xenon, argon, and neon. As predicted from the two-state model, the shift in T_{melt} is larger for LJ_{55}, which has a higher average vibrational frequency in its icosahedral global minimum, than for other nonmagic sizes.

The heat capacity of Ne_{19} shows the same variations in the melting point as the path-integral MC simulations of Chakravarty.[6] The heights of the peaks are too low, and indicate that the anharmonic terms are significant. However, given the size of the error bars and how far the classical results reported in Ref. 6 are from other published data,[50] we think that the agreement found for this cluster is very satisfactory.

The very low temperature at which the structural transition takes place in LJ_{31} makes this cluster sensitive to quan-

Downloaded 25 May 2001 to 131.111.112.18. Redistribution subject to AIP license or copyright, see http://ojps.aip.org/jcpo/jcpcr.jsp

tum effects. Even a very low value of the de Boer parameter is enough to make the small heat capacity peak disappear, and Xe_{31} only displays a bump at $T \sim 0.03\,\varepsilon/k_B$. Surprisingly, Ar_{31} and Ne_{31} both exhibit a very sharp peak at even lower temperatures. These effects result from changes in the global minimum, and will be examined further in the next section.

The preliminary icosahedral transition in LJ_{38} also occurs at a relatively low temperature, near $0.1\,\varepsilon/k_B$, but the melting peak itself is located at $T \sim 0.17\,\varepsilon/k_B$. Such low temperatures make the caloric curve extremely dependent on Λ for this cluster, and the small bump indicative of premelting is no longer visible for argon. The effect on neon is even stronger, no peak remaining visible at all in the temperature range $0 < T < 0.5\,\varepsilon/k_B$.

No structural transition or premelting effects complicate the caloric curve of LJ_{55}, and so the melting peak is much clearer. As with smaller clusters, we notice that quantum delocalization is already non-negligible for argon below the melting point. Anharmonic corrections would probably raise all the curves of Fig. 6, but the shift in the latent heats from the classical result should be roughly unchanged. The data obtained for this cluster and for the smaller 13-atom cluster can be used within the framework of the two-state model to predict approximate values of the shifts in the melting temperature of larger clusters. The two-state model is expected to be a reasonable description of magic clusters especially at large sizes. In a first approximation, we write all variables in Eq. (12) as asymptotic expansions to first order in $n^{-k/3}$. Thus the shift in the melting temperature induced by quantum delocalization can be expressed simply as a two-parameter function, for a given value of h,

$$\Delta T(n) = \Delta T(\infty)[1 + a n^{-1/3} + O(n^{-2/3})]. \tag{30}$$

In this equation, the shift in the bulk melting point $\Delta T(\infty)$ is

$$\Delta T(\infty) = -\frac{h^2}{8L}(\nu_S^{\mathrm{rms}}(\infty) - \nu_L^{\mathrm{rms}}(\infty))(\nu_S^{\mathrm{rms}}(\infty) + \nu_L^{\mathrm{rms}}(\infty)), \tag{31}$$

where L is the latent heat of melting. The application of Eq. (30) to the clusters Ne_{13} and Ne_{55} allows us to estimate the approximate values of the shift ΔT for larger neon clusters and for the bulk limit. We find $\Delta T(147) = 1.6\,\mathrm{K}$ and $\Delta T(\infty) = 2.0\,\mathrm{K}$.

B. Stability diagrams

In her study of quantum delocalization on cluster melting, Chakravarty[7] showed that melting could be induced either by increasing Λ at fixed temperature, or by increasing T at fixed Λ. Fixing the temperature and varying the degree of quantum delocalization for a prescribed system may not seem a very physical procedure, but it allows the different effects to be studied separately. Because she performed path-integral MC simulations, Chakravarty was limited to a small set of values for Λ and T. Additionally, she used the Lindemann index as a probe of melting, which is not suitable for complex systems such as LJ_{31} or LJ_{38} because of preliminary transitions.[35]

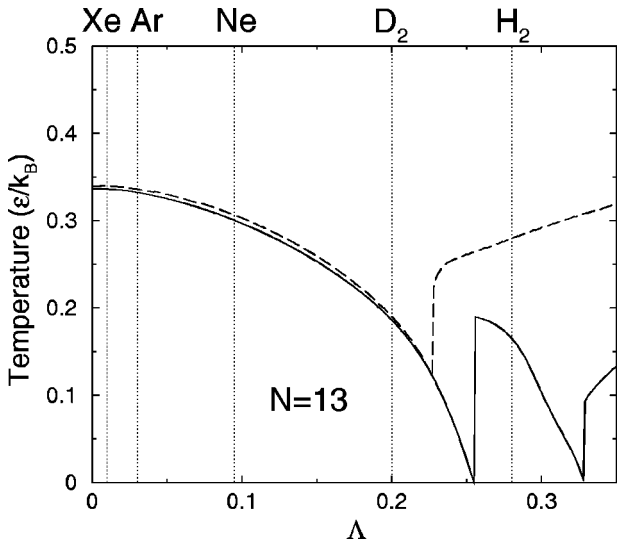

FIG. 7. Diagram of stability of LJ_{13} as a function of quantum delocalization. The solid line is the freezing curve, the dashed line is the melting curve. The five vertical lines indicate the values of the de Boer parameter Λ for Xe, Ar, Ne, D_2, and H_2, respectively.

We have used the present quantum superposition method to quantify the influence of delocalization on the thermodynamics of the five clusters investigated above. As a definition of the melting temperature, we have chosen the position of the heat capacity peak. When the peak disappears due to strong delocalization, we relied on an alternative, more subjective definition, namely the temperature where the highest 99% of minima (in energy) become dominant, i.e., their occupation probability exceeds 50%. Because we used two possible definitions for the melting temperature, its value may jump when a peak in the heat capacity appears or vanishes. The freezing temperature was simply taken as the temperature above which the global minimum is no longer dominant. These definitions can account, in a first approximation, for coexistence phenomena and the possibility of two-step melting.

We have represented in Fig. 7 the stability diagram obtained for LJ_{13} in the range $0 \leqslant \Lambda \leqslant 0.35$. The lower part of this diagram, below the freezing curve, shows the region of stability of the ''pure'' solidlike phase corresponding to the global minimum alone, while the upper part, above the melting curve, shows the region of stability of the liquidlike phase and its numerous minima. As can be seen from this figure, the two lines coincide from the classical regime up to about $\Lambda \simeq 0.25$, the value at which the heat capacity peak vanishes. This coincidence reflects the two-state character of this system. In the quasiclassical regime, the melting temperature roughly decreases with Λ as Λ^2, in agreement with semiclassical expansions. The most striking features in this diagram are the points at which the freezing curve meets the $T = 0$ line. This is because the minimum with the lowest value of E_α^0 can change as a function of Λ. Larger values of Λ favor those minima with a lower arithmetic mean vibrational frequency, because they have a lower zero-point energy. As Fig. 7 illustrates, there can be several changes in the global minimum with Λ. More precisely, the existence of

Downloaded 25 May 2001 to 131.111.112.18. Redistribution subject to AIP license or copyright, see http://ojps.aip.org/jcpo/jcpcr.jsp

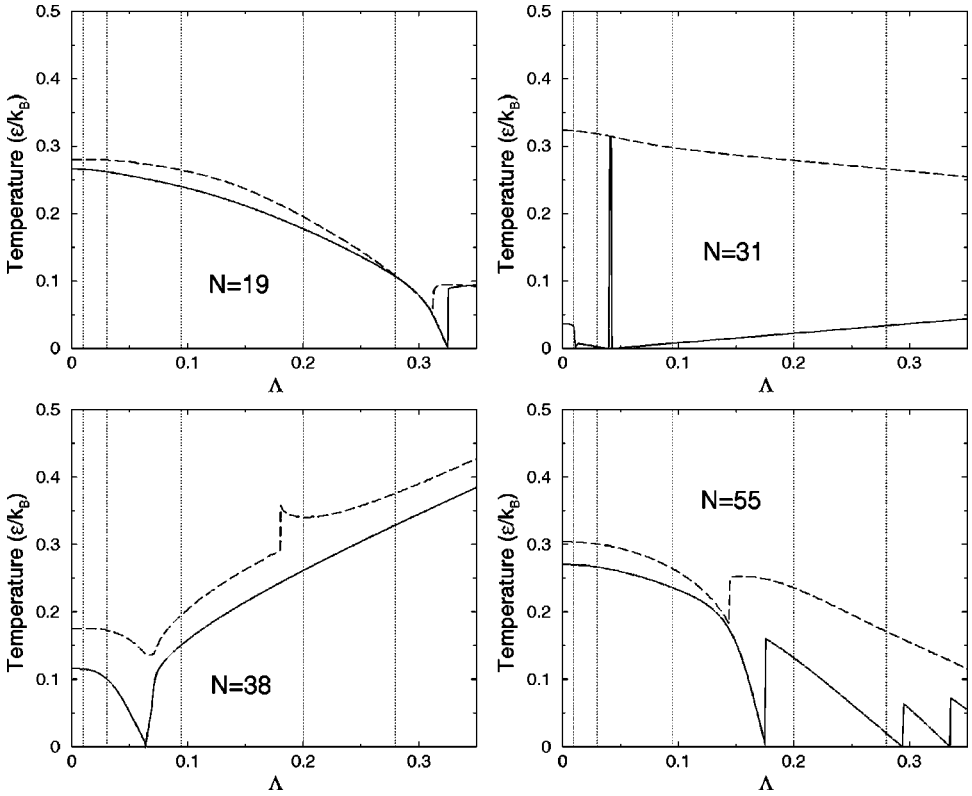

FIG. 8. Diagrams of stability of LJ_{19}, LJ_{31}, LJ_{38}, and LJ_{55} as a function of the de Boer parameter Λ. The solid line is the freezing curve, the dashed line is the melting curve. Vertical lines are the same as in Fig. 7.

such changes in morphology can be checked from the database of minima by simply looking at the values of

$$\Lambda_{\alpha_0}=\min_{\alpha}\left\{\frac{2}{\kappa}\left(\frac{E_\alpha-E_{\alpha_0}}{\langle\nu_\alpha\rangle-\langle\nu_{\alpha_0}\rangle}\right),\ \langle\nu_\alpha\rangle>\langle\nu_{\alpha_0}\rangle\right\}. \tag{32}$$

If α_0 is the classical global minimum, and if Λ_{α_0} exists and is positive, then the global minimum changes when Λ crosses Λ_{α_0} to the isomer α that minimizes Λ_{α_0}. Further changes in the global minimum can be estimated in the same way. Two such crossovers are found in the database for LJ_{13}, respectively located at $\Lambda=0.255$ and $\Lambda=0.328$, in complete agreement with the results shown in Fig. 7. Thus this simple diagram shows for instance that the geometries of $(D_2)_{13}$ and $(H_2)_{13}$ should differ strongly owing to the difference in zero-point energy. Actually, this result is in agreement with previous PIMC works on the thermodynamics of these two systems showing that $(H_2)_{13}$ has a liquidlike phase at temperatures where $(D_2)_{13}$ is still rigidlike.[51] In particular, Scharf *et al.* have shown that the icosahedral structure of $(H_2)_{13}$ was only marginally stable at $T=2.5\,\mathrm{K}$, the cluster exhibiting most frequently very disordered geometries.[52]

Similar stability diagrams for the four larger clusters are shown in Fig. 8. The general picture resembles that for LJ_{13}, with a quadratic decrease in the melting and freezing temperatures in the quasiclassical regime, and some changes in the global minimum as quantum delocalization increases.

The structure of the 19-atom cluster appears to be the most resistant to quantum effects, as it only shows one crossover at $\Lambda=0.325$ in the range $\Lambda\leqslant 0.35$. The coexistence range $\Delta T=T_{\mathrm{melting}}-T_{\mathrm{freezing}}$ is larger than for LJ_{13}, and remains of this magnitude up to the strong quantum delocalization regime of $\Lambda\simeq 0.2$.

LJ_{31} is probably the most intriguing case studied here, as it undergoes three consecutive changes in the global minimum associated with qualitative changes in the low-temperature heat capacity curves (see above). The three crossovers occur at $\Lambda=0.011$, 0.040, and 0.043, and involve surface rearrangements towards anti-Mackay geometries. The Mackay/anti-Mackay transition is therefore favored by both temperature effects and by quantum delocalization. One of these three isomers entropically dominates over the others, and corresponds to the solidlike state that is stable up to the melting point when it becomes the effective global minimum $(0.040<\Lambda<0.043)$.

LJ_{38} shows only one crossover at $\Lambda=0.065$. Such a low value probably explains why the heat capacity of Ne_{38} is so qualitatively different from that of Ar_{38}. Looking at the caloric curves near this crossover shows that the melting peak disappears above this value, and only reappears at $\Lambda\simeq 0.18$. This explains the discontinuity in the melting temperature on the diagram of this cluster.

LJ_{55} also shows three changes in its global minimum as quantum effects rise, namely at $\Lambda=0.175$, 0.294, and 0.335. As for the smaller icosahedron LJ_{13}, these changes are facilitated by the large vibrational frequencies of the high symmetry ground state, which are not compensated by the difference in potential energies. For this size, Ne_{55} and $(D_2)_{55}$ are predicted to have different morphologies.

The results of these stability diagrams show a strong dependence on the vibrational properties of the cluster. Be-

Downloaded 25 May 2001 to 131.111.112.18. Redistribution subject to AIP license or copyright, see http://ojps.aip.org/jcpo/jcpcr.jsp

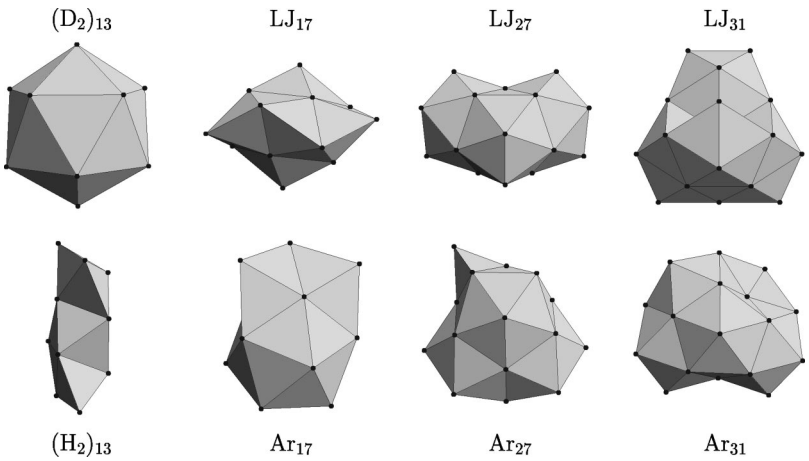

FIG. 9. Structures of some clusters that exhibit a change in the global potential energy minimum due to quantum delocalization.

cause we used only incomplete samples of minima, one may wonder whether other isomers that are not included in our sample could be lower in energy at some degree of delocalization. All curves in Fig. 8 have been checked twice, and the same new global minima were found from the two independently generated databases. Nevertheless, this sensitivity of cluster structure in the quantum regime to the vibrational frequencies merits further investigation.

VI. LOW-TEMPERATURE BEHAVIOR AND DEBYE TEMPERATURES

All isomers found as new global minima of the effective quantum potential were discovered by classical simulations performed to estimate the respective weights in the partition functions. We have also assumed that the weights in the quantum partition function would be unchanged from the classical weights, but this is not true for the partition functions themselves, which are far more influenced by the vibrational properties in the quantum case. In order to analyze the influence of delocalization on cluster structure, it is thus important to include the quantum character during the search for possible lowest-energy structures.

A. Global optimization of Lennard-Jones clusters including quantum delocalization

We have used the basin-hopping Monte Carlo algorithm[53,54] to explore the energy landscape of LJ_n clusters in the size range $n \leqslant 100$, and to find the global minima as a function of the de Boer parameter Λ. After each quench was performed, the zero-point energy contribution was added to the potential energy, and the Metropolis acceptance probability was calculated using these effective quantum energies. Since the diagonalization of the Hessian matrix involved in the calculation of the vibrational frequencies is computationally demanding, especially for large clusters, we started the optimizations from the classical global minimum for each n. 5000 quenches were performed for each size, at the temperature $T=1.5\varepsilon/k_B$ and with $\Lambda=0.095$. We are aware that 5000 is a relatively small number, which may be inadequate to find the true global minimum for sizes larger than $n>50$. However, this initial survey will give us insight into the extent to which rare-gas clusters can be considered as classical from a static point of view.

In the size range $n \leqslant 100$, Lennard-Jones clusters preferentially exhibit icosahedral-based geometries, with different possible external arrangements.[54,55] Only a few sizes have been shown to deviate from this icosahedral sequence, at $n=38$ (truncated octahedron), $n=75-77$ (Marks' decahedra), and $n=98$ (tetrahedral structure).[56] The effect of quantum delocalization is quantified in Table I, where we report the best energies found and compare them with the LJ global minimum. These global minima are available at the Cambridge Cluster Database.[57] Neon, of course, is most influenced by quantum effects, and shows a different global minimum in 35 out of the 99 cases investigated. However, Ar_n is also seen to differ from the classical LJ_n for a few sizes, including 17, 27, and 31, but also the larger 76- or 77-atom clusters where the icosahedral minima are preferred to the decahedral geometries. Krypton clusters, not included in this table, sometimes also show differences from the classical structure. Xenon clusters differ from the purely classical Lennard-Jones prediction in only three cases ($n=65$, 86, and 98). Although challenging, it would be interesting to verify these results with more accurate quantum Monte Carlo calculations at $T=0$. A reasonable test case could be the size $n=17$, where three different effective global minima are found, depending on the degree of delocalization.

Not surprisingly, most of the structural changes displayed by these clusters arise from different arrangements of the outer layer, and take place for sizes where the Mackay and anti-Mackay overlayers compete:[55] between $n=25$ and $n=35$, near $n=67$, and near $n=88$. Differences between the classical and quantum gometries are illustrated in Fig. 9 for some selected sizes. In the case of the 13-atom cluster, we have shown how the global minimum structures of $(D_2)_{13}$ and $(H_2)_{13}$ are expected to differ, even though the icosahedron remains as the global minimum for rare gases. The very prolate shape of $(H_2)_{13}$ induces some floppy vibrational modes, thus lowering the average frequency and zero-point energy. We also show the different isomers of LJ_n and Ar_n for $n=17$, 27, and 31. Including delocalization usually makes the structure much more distorted, as was noticed by Hodgdon and Stillinger in the case of solid helium.[27] Our study of neon clusters shows that most new global minima have only C_1 symmetry. For all these sizes, we expect sig-

Downloaded 25 May 2001 to 131.111.112.18. Redistribution subject to AIP license or copyright, see http://ojps.aip.org/jcpo/jcpcr.jsp

TABLE I. Lennard-Jones clusters LJ_n which change global minimum in the range $n \leqslant 100$. Energies are given in units of ϵ. For each size and species, the global minimum is underlined.

Size	LJ ($\Lambda=0$)	Xe ($\Lambda=0.01$)	Ar ($\Lambda=0.03$)	Ne ($\Lambda=0.095$)	Point group	Size	LJ ($\Lambda=0$)	Xe ($\Lambda=0.01$)	Ar ($\Lambda=0.03$)	Ne ($\Lambda=0.095$)	Point group
17	−61.317 99	−58.670 10	−53.374 32	−36.163 03	C_2	69	−359.664 32	−345.964 85	−318.565 91	−229.519 37	C_1
17	−61.307 15	−58.666 63	−53.385 58	−36.222 20	C_1	72	−378.637 25	−364.252 11	−335.481 81	−241.978 35	C_s
17	−61.296 77	−58.658 69	−53.382 52	−36.235 00	C_{3v}	72	−378.523 99	−364.162 54	−335.439 63	−242.090 19	C_1
27	−112.873 58	−108.393 26	−99.432 60	−70.310 47	C_{2v}	75	−397.492 33	−382.110 32	−351.346 29	−251.363 20	D_{5h}
27	−112.825 52	−108.363 45	−99.439 33	−70.435 91	C_s	75	−396.238 51	−381.246 30	−351.261 87	−253.812 49	C_1
28	−117.822 40	−113.178 88	−103.891 84	−73.708 96	C_s	76	−402.894 87	−387.323 95	−356.182 12	−254.971 17	C_s
28	−117.777 96	−113.152 75	−103.902 33	−73.838 47	C_s	76	−402.384 58	−387.158 78	−356.707 20	−257.739 53	C_1
30	−128.286 57	−123.283 48	−113.277 30	−80.757 21	C_{2v}	76	−401.862 14	−386.705 54	−356.392 30	−257.874 37	C_1
30	−128.181 59	−123.194 82	−113.221 27	−80.807 23	C_{2v}	77	−409.083 52	−393.276 96	−361.663 83	−258.921 18	C_{2v}
31	−133.586 42	−128.104 41	−117.140 38	−81.507 30	C_s	77	−408.518 27	−393.064 35	−362.156 53	−261.706 11	C_1
31	−133.293 82	−128.097 68	−117.705 40	−83.930 50	C_1	77	−408.155 37	−392.785 36	−362.045 34	−262.140 29	C_1
31	−133.104 62	−127.954 44	−117.654 09	−84.177 93	C_1	78	−414.794 40	−399.098 29	−367.706 07	−265.681 37	C_s
32	−139.635 52	−133.928 25	−122.513 70	−85.416 42	C_{2v}	78	−414.442 51	−398.840 30	−367.635 87	−266.221 48	C_1
32	−138.823 61	−133.497 88	−122.846 41	−88.229 15	C_{2v}	79	−421.810 90	−405.876 42	−374.007 45	−270.433 32	C_1
33	−144.842 72	−138.930 97	−127.107 48	−88.681 12	C_s	79	−420.709 75	−404.896 48	−373.269 93	−270.483 64	C_1
33	−143.622 17	−138.129 74	−127.144 87	−91.444 05	C_1	82	−440.550 43	−423.817 38	−390.351 29	−281.586 50	C_1
34	−150.044 53	−143.928 54	−131.696 58	−91.942 68	C_{2v}	82	−440.041 39	−423.532 48	−390.514 66	−283.206 72	C_1
34	−148.351 36	−142.673 75	−131.318 53	−94.414 04	C_1	83	−446.924 09	−429.963 30	−396.041 72	−285.796 58	C_{2v}
35	−155.756 64	−149.429 00	−136.773 70	−95.644 00	C_1	83	−445.800 65	−429.102 37	−395.705 80	−287.166 98	C_1
35	−153.695 48	−147.870 74	−136.221 27	−98.360 49	C_s	84	−452.657 21	−435.480 96	−401.128 44	−289.482 76	C_1
36	−161.825 36	−155.273 06	−142.168 46	−99.578 49	C_s	84	−451.650 41	−434.761 88	−400.984 82	−291.209 37	C_1
36	−158.676 22	−152.648 41	−140.592 81	−101.412 08	C_s	85	−459.055 80	−441.819 40	−407.346 60	−295.310 00	C_1
37	−167.033 67	−160.277 16	−146.764 13	−102.846 79	C_1	85	−457.954 41	−440.834 85	−406.595 72	−295.318 55	C_1
37	−163.873 63	−157.602 17	−145.059 25	−104.294 74	C_1	86	−465.384 49	−447.751 72	−412.486 17	−297.873 15	C_1
38	−173.928 43	−166.828 35	−152.628 18	−106.477 65	O_h	86	−465.237 87	−447.826 34	−413.003 29	−299.828 36	C_1
38	−168.519 99	−162.088 87	−149.226 62	−107.424 31	C_1	87	−472.098 16	−454.225 68	−418.480 72	−302.309 59	C_1
44	−207.688 73	−199.416 47	−182.871 97	−129.102 32	C_1	87	−471.383 20	−453.801 46	−418.637 98	−304.356 68	C_1
44	−203.861 02	−196.048 03	−180.422 07	−129.637 67	C_1	88	−479.032 63	−460.904 78	−424.649 07	−306.818 04	C_1
57	−288.342 62	−277.186 18	−254.873 28	−182.356 36	C_s	88	−476.631 77	−458.863 00	−423.325 46	−307.828 46	C_1
57	−288.259 86	−277.113 22	−254.819 94	−182.366 78	C_s	89	−486.053 91	−467.688 76	−430.958 44	−311.584 93	C_1
65	−334.971 53	−322.101 10	−296.360 23	−212.702 42	C_1	89	−482.836 55	−464.846 32	−428.865 87	−311.929 39	C_1
65	−334.969 70	−322.104 87	−296.375 22	−212.753 84	C_1	92	−505.185 31	−486.139 99	−448.049 37	−324.254 82	C_1
65	−334.402 50	−321.598 41	−295.990 23	−212.763 65	C_1	92	−502.366 42	−483.651 37	−446.221 29	−324.573 52	C_1
66	−341.110 60	−328.017 25	−301.830 55	−216.723 78	C_1	93	−510.877 69	−491.613 96	−453.086 52	−327.872 31	C_1
66	−340.763 60	−327.728 73	−301.658 99	−216.932 34	C_1	93	−507.488 68	−488.680 53	−451.064 25	−328.811 32	C_1
67	−347.252 01	−333.930 58	−307.287 73	−220.698 48	C_s	98	−543.665 36	−523.066 51	−481.868 80	−347.976 26	T_d
67	−347.049 76	−333.796 75	−307.290 74	−221.146 20	C_1	98	−543.642 96	−523.203 37	−482.324 20	−349.466 88	C_s
69	−359.882 57	−346.136 91	−318.645 61	−229.298 87	C_1						

nificant differences in the dynamical and thermodynamic behavior in the quantum regime, even at reasonably high temperatures.

A comparison of the present results with the experimental data of Märk and Scheier[58] is quite difficult, because the mass spectra obtained by these authors for neutral neon clusters do not show a clear picture of the magic numbers. However, the results of Harris *et al.*[59] for argon clusters clearly indicate that the anti-Mackay sequence is stable up to the size $n=34$. Quantum delocalization shifts the crossover between the anti-Mackay and Mackay sequences to $n=34$, although Ar_{34} has a Mackay-type geometry. This small discrepancy would probably be resolved by using a more accurate argon potential than the basic Lennard-Jones model.

B. Debye temperatures of argon clusters

For a three-dimensional *continuous* solid, the Debye approximation[60] models the vibrational density of states g as a quadratic function of ν with a cutoff at $\nu_{\max}$: $g(\nu) \propto \nu^2 \Theta(\nu_{\max}-\nu)$, where Θ is the step function. The resulting formula for the total heat capacity is

$$C_v^{\text{Debye}}(T) = 3\kappa k_B \left(\frac{T}{T_D}\right)^3 \int_0^{T_D/T} \frac{x^4 e^x}{(e^x-1)^2}\, dx, \tag{33}$$

where the Debye temperature T_D is related to $\nu_{\max}$ by $h\nu_{\max}=k_B T_D$. This formula contrasts with the corresponding expression for a *discrete* solid,

$$C_v(T) = k_B \sum_{i=1}^{\kappa} \left(\frac{h\nu_i}{k_B T}\right)^2 \frac{e^{h\nu_i/k_B T}}{(e^{h\nu_i/k_B T}-1)^2}. \tag{34}$$

In particular, the behavior at low temperature is different, although both models converge to the Dulong–Petit Law at high T. Attributing a Debye temperature to a cluster may seem strange at first sight, since the structures we consider are still far from the continuum. However, the Debye formula (33) is just an interpolation made to account for the observed Dulong–Petit behavior at high temperatures, as

Downloaded 25 May 2001 to 131.111.112.18. Redistribution subject to AIP license or copyright, see http://ojps.aip.org/jcpo/jcpcr.jsp

TABLE II. Parameters of the asymptotic expansion (35) for the icosahedral (ICO), decahedral (DEC), and truncated octahedral (TOCT) growth sequences.

Sequence	$T_D(\infty)$ (K)	a	b	c
ICO	87.304	−1.229	0.445	0.932
DEC	88.730	−1.271	0.625	0.571
TOCT	88.788	−1.295	0.759	0.607

well as the observed T^3 dependence near $T=0$. Therefore, there is no fundamental problem with the use of Eq. (33) as an approximation to Eq. (34).

In order to estimate the Debye temperatures of LJ clusters with some degree of quantum delocalization, we have fitted the ''exact'' heat capacity of Eq. (34) to a Debye form (33) by a standard least-squares method. Such a procedure requires several comments. First we must ensure that the isomer we consider is indeed the one corresponding to the ''solid'' state. Hence the structures should be selected according to their effective quantum energies including the zero-point contribution. Second, melting points in clusters are usually much lower than the bulk melting point. Consequently, the neglect of all isomers except the global minimum may not reproduce the actual caloric curve if the degree of quantum delocalization is high (neon), or if some preliminary transitions or premelting phenomena are present (e.g., LJ_{31}). In these cases, the heat capacity of the solidlike isomer alone will underestimate the real heat capacity. However, a fit to a Debye law would also be meaningless if some extra bumps or peaks are apparent. To avoid this problem, we have focussed on clusters having only a modest quantum character, namely argon clusters.

We estimated the Debye temperature of all Ar_n clusters in the range $3 \leqslant n \leqslant 100$ using the putative global minima determined previously. In the range $101 \leqslant n \leqslant 150$, a similar investigation was made by assuming that the geometries of Ar_n are the same as those of LJ_n. Finally, we considered three growth sequences in the large size regime, namely, icosahedral (ICO), decahedral (DEC), and truncated octahedral (TOCT), for which we fitted the measured values of T_D according to the simple asymptotic expansion,

$$T_D(N) = T_D(\infty)[1 + aN^{-1/3} + bN^{-2/3} + cN^{-1}]. \qquad (35)$$

Clusters as large as $n=10179$ (ICO), $n=9062$ (DEC), and $n=9201$ (TOCT) were used to obtain the coefficients $T_D(\infty)$, a, b, and c for each sequence. The results of the fits are reported in Table II. They probably underestimate the bulk Debye temperature $T_D(\infty)$, because 9000 atoms is still a relatively small size, and also because several rather small sizes such as $n=13$ (ICO), $n=18$ (DEC), or $n=38$ (TOCT) are included in the fit.

The variation of the estimated Debye temperature with size for solid argon clusters is shown in Fig. 10. The nonmonotonic variations in the small size regime $n \lesssim 100$ are characteristic of cluster size effects,[61] as opposed to the much smoother and regular variations above this limit. Even though we did not systematically study sizes above 150 apart from growth sequences, we do not expect drastic changes for this kind of cluster, at least not of the same magnitude as those observed near the anti-Mackay/Mackay crossover at $n=34$. At this size, the cluster changes shape, gains more potential energy than it loses zero-point energy, and by increasing its vibrational energy its Debye temperature also increases.

The agreement between the bulk Debye temperature estimated from extrapolating Eq. (35) to $n \to \infty$ and the experimental bulk value of 92 K is quite good. The remaining discrepancy could probably be reduced by replacing the rather crude Lennard-Jones model by more accurate potentials for argon, by including anharmonic corrections to the heat capacities, and also by fitting Eq. (35) using larger clusters of the most stable sequence, namely, the truncated octahedron.

The correlation between the Debye temperature and the cluster structure is made via the vibrational spectrum, but for very ordered large clusters ($n>150$) the present results seem to indicate only small changes in the Debye temperatures for different sequences. However, disordered geometries or clusters trapped in metastable isomers may have significantly different vibrational properties, which may have a measurable effect on the thermal behavior. We have compared the Debye temperatures of a 201-atom cluster in its very ordered TOCT geometry and in an amorphous state. This latter state was made of 100 geometries quenched from random starting points, whose contributions were added using the superposition method. The heat capacities are plotted in the upper panel of Fig. 11, together with the corresponding vibrational densities of states (DOS) in the lower panel. We also plotted the equivalent Debye DOS of the ordered cluster for comparison.

Clearly, the Debye approximation is only realistic for the nearly crystalline cluster and fails for the amorphous state. The presence of many soft modes in the amorphous state decreases the Debye temperature by about 5 K with respect to the TOCT structure. The vibrational DOS of the truncated octahedral cluster is rather far from its equivalent Debye distribution, despite the fact that the corresponding heat capacities are very close to each other. This gives us an idea of how

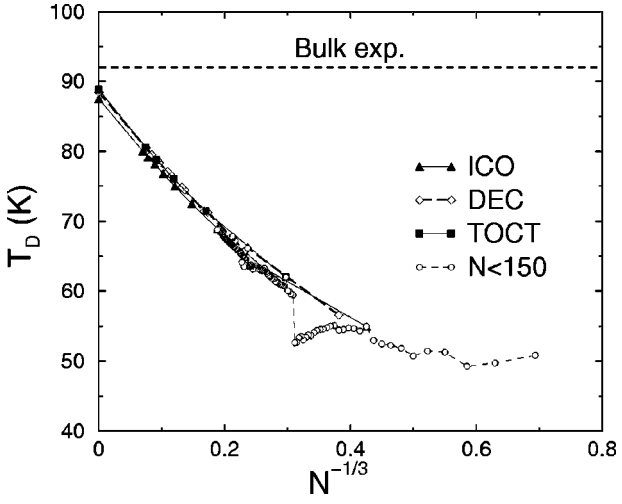

FIG. 10. Variations in the Debye temperature of argon clusters with size.

Downloaded 25 May 2001 to 131.111.112.18. Redistribution subject to AIP license or copyright, see http://ojps.aip.org/jcpo/jcpcr.jsp

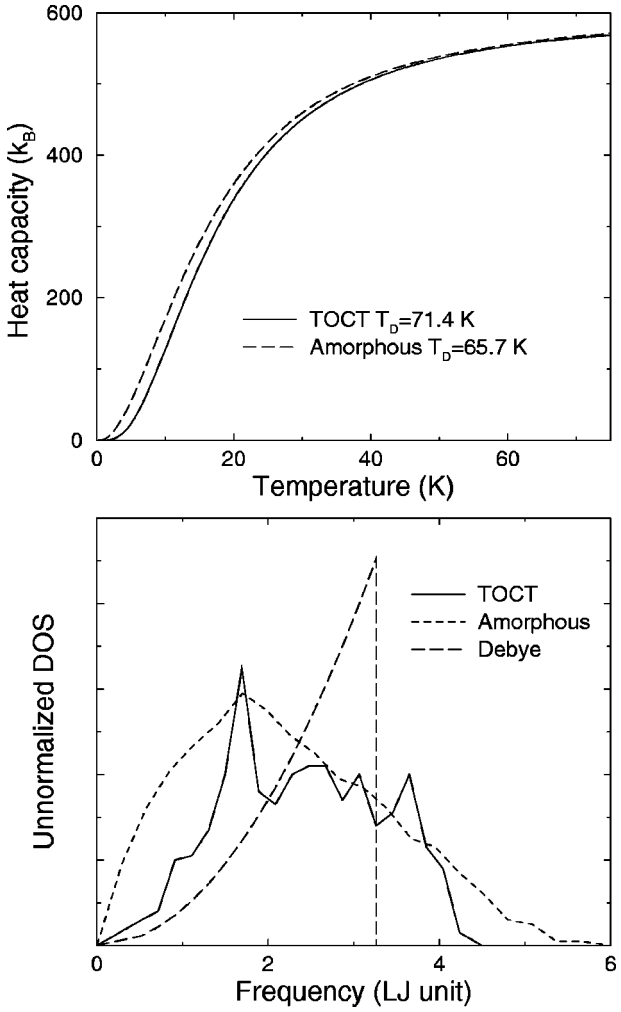

FIG. 11. Upper panel: heat capacities of a crystalline Ar_{201} cluster (TOCT) and for a sample of 100 amorphous minima. Lower panel: corresponding vibrational densities of states. The Debye density of states is the equivalent distribution for the TOCT cluster at the Debye temperature.

far we are from the continuum limit for a cluster of 201 atoms. Inspecting the DOS for larger clusters shows that the ν^2 law is still approximate even for 9201 atoms, because the variations of $g(\nu)$ are strongly nonmonotonic. On the other hand, the smooth vibrational DOS displayed by the amorphous structures is in fact little affected by the averaging procedure, and is nearly the same for all the individual amorphous minima considered in the sample. No evidence for linear variations of the heat capacity as $T \rightarrow 0$ was found in Fig. 11, which would be a signature of glassy behavior. A proper treatment of this regime would, however, probably require a method that, unlike the superposition approach, does not ignore tunneling.

VII. CONCLUSION

In this work, we have investigated the low temperature thermodynamics of rare-gas clusters using several different methods. The development of effective potentials from condensed matter physics provides a computationally convenient way to include quantum corrections in a semiclassical framework. We have used the quadratic Feynman–Hibbs potential and the Fujiwara–Osborn–Wilk potential based on the Wigner–Kirkwood expansion, both potentials being truncated at first order in $\hbar^2$. These potentials were tested on the melting of the 13-atom Lennard-Jones cluster with different degrees of quantum delocalization. The Feynman–Hibbs effective potential has been shown to reproduce the results of more accurate path-integral Monte Carlo simulations surprisingly well, down to temperatures where the quantum calculations become rather expensive. In particular, it gives a correct account of the decrease in the latent heat and melting point in Ne_{13}. On the other hand, the potential based on the Wigner–Kirkwood expansion suffers from numerical problems that make it unsuitable (in its simple form) for studying the dynamics of clusters in a wide temperature range including both the solidlike and liquidlike states. Both effective potentials were found to be inadequate at very low temperatures.

To correct for the deficiencies of the effective potentials, we have extended the harmonic superposition method to the quantum regime by considering quantum harmonic partition functions. This idea was tested first on the simple two-state model, which showed the general influence of the vibrational properties on the most stable structure and the melting point. Its extension to a sample of minima on an energy landscape was seen to give good agreement with path-integral MC simulations of Ne_{13}. For larger sizes, we used a reweighting technique to account for the incomplete sample, similar to that previously used in a classical context.[21] We presented a quasiclassical version of the superposition method, and we also extended the quantum version to include anharmonic corrections to the partition function, which gives quantitative agreement with the caloric curve of Ne_{13}.

Using the quantum superposition method we have studied the effects of delocalization on the melting and premelting of 19-, 31-, 38-, and 55-atom LJ clusters. We observed a general decrease of the latent heat and melting point. This decrease is largest for the magic number Ne_{55} cluster, confirming the prediction of the two-state model that tightly bound systems should be less resistant to heating. Using the results for Ne_{13} and Ne_{55} in the framework of the two-state model, we have estimated the bulk contribution of quantum delocalization to the melting point to be roughly 2 K. Clusters exhibiting preliminary structural transitions in the classical regime, such as LJ_{31} and LJ_{38}, are strongly affected by quantum delocalization, as they are more likely to have a change in the global minimum. These effects have been rationalized by calculating stability diagrams where the melting and freezing temperatures are plotted against the de Boer parameter, which quantifies the amount of delocalization.

We then focused on the very low temperature properties by looking more systematically at the effect of delocalization on cluster structure. Our simple approach shows that the classical LJ potential is too crude for describing neon clusters when surface rearrangements occur. We estimated the Debye temperatures of argon clusters over a wide size range and for several growth sequences. The size-dependence displays nonmonotonic variations characteristic of cluster size effects, which are especially strong near the anti-Mackay/Mackay crossover. The influence of cluster structure on the

Downloaded 25 May 2001 to 131.111.112.18. Redistribution subject to AIP license or copyright, see http://ojps.aip.org/jcpo/jcpcr.jsp

Debye temperature was further investigated by comparing the behavior of a symmetrical, truncated octahedral 201-atom cluster and a set of amorphous isomers. A much lower Debye temperature was found in the latter case, although there is no reason why the continuous approximation should work at such low sizes.

The quantum harmonic superposition method developed in this work is a complementary approach to path-integral simulations. It is predictive down to arbitrary low temperatures, and works best as the temperature decreases, because fewer isomers contribute to the partition function and because the harmonic approximation improves. Most importantly, this approach uses only parameters from classical simulations, which makes it suitable for much larger sizes, or more complex systems exhibiting quasiergodicity. Its predictions can be made quantitative by incorporating anharmonic corrections in a simple way, choosing appropriate values of the newly introduced parameters to reproduce the results of classical simulations. The method is especially powerful as it allows the calculation of thermal properties in continuous ranges of temperature and for any degree of quantum delocalization. Its main approximation, besides the harmonic assumption, is to neglect tunneling. It could be used to study other finite systems, as well as bulk liquids or glasses beyond the classical regime. One major improvement to the method could be the incorporation of self-consistent harmonic theories such as the the ones developed by Voth and co-workers.[18,19] In particular, we believe that the precise calculation of effective normal modes could be used to remove the unknown anharmonicity parameters of the present theory, in both the classical and quantum cases. We are currently working along these lines.

The experimental measurement of Debye temperatures in clusters has recently been accomplished by the Haberland group for sodium.[62] In view of the peculiarities of thermodynamic size effects in alkali clusters,[63] we expect even more intricate variations of the Debye temperature than those observed here for argon clusters. In this respect, we believe that the tools and results presented here provide a very promising way of including quantum effects in the finite-temperature study of complex many-body systems beyond the approximation of effective potentials.

ACKNOWLEDGMENTS

This research has been supported by a Marie Curie Fellowship of the European Community program ''Improving Human Research Potential and the Socio-Economic Knowledge Base'' under Contract No. HPMFCT-2000-00598. F.C. acknowledges helpful discussions with Martin Schmidt, and the diagonalization of large Hessian matrices by Sylvain Capponi. J.P.K.D. is grateful to Emmanuel College for the award of a research fellowship.

APPENDIX A: GAUSSIAN FEYNMAN–HIBBS EFFECTIVE POTENTIAL FOR LJ SYSTEMS

The analytic calculation of the Gaussian effective potential, Eq. (1), can be performed for an interaction potential which is decomposed into a sum of Gaussian functions. For the Lennard-Jones potential, we use a simple 2-term decomposition,[64]

$$V_{\mathrm{LJ}}(r) \approx \sum_k \gamma_k \exp(-\alpha_k r^2), \tag{A1}$$

with parameters taken from Ref. 64: $\gamma_1 = 14\,487.1$, $\gamma_2 = -5.553\,38$, $\alpha_1 = 9.051\,48$, and $\alpha_2 = 1.225\,36$. Inserting the above expression into Eq. (1) leads to the following effective pairwise Feynman–Hibbs potential:

$$v_{\mathrm{GFH}}(r,\beta) = \sum_k \gamma_k \chi_k^3 \exp(-\alpha_k \chi_k r^2), \tag{A2}$$

where the coefficient χ_k is

$$\chi_k(\beta) = \left(1 + \frac{\alpha_k \beta \hbar^2}{3m}\right)^{-1}. \tag{A3}$$

A standard simulation can then be performed with this potential, and the thermal properties calculated in the usual way. We plot in Fig. 12 the heat capacity calculated from Eq. (5) for Xe_{13}, Ar_{13}, and Ne_{13}. Except for neon, the curves are almost identical to the results obtained with the quadratic FH potential in Fig. 1. For Ne_{13} we find that the Gaussian effective potential is a worse approximation than the quadratic potential, in comparison to the path-integral results of Neirroti, Freeman, and Doll.[5] However, it is difficult to state precisely the origin of this larger discrepancy, because of the approximation involved in the Gaussian decomposition of the LJ potential.

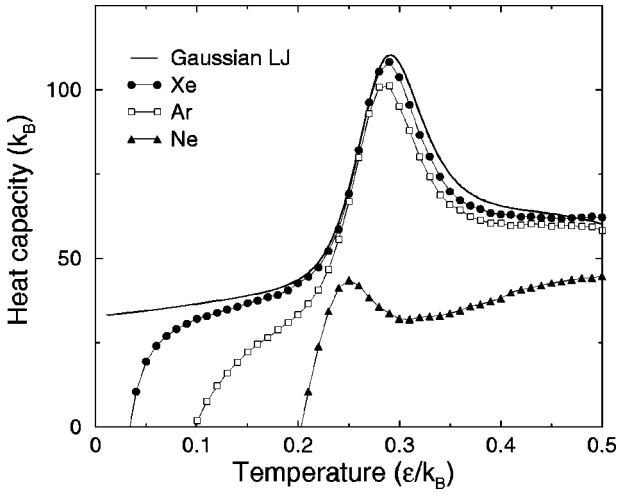

FIG. 12. Heat capacities of LJ_{13} clusters at various degrees of quantum delocalization, calculated from Monte Carlo simulations using the Gaussian decomposed LJ (GLJ) potential and effective Gaussian Feynman–Hibbs quasiclassical potentials. Results are shown for the classical case ($\Lambda = 0$), for xenon ($\Lambda = 0.01$), argon ($\Lambda = 0.03$), and neon ($\Lambda = 0.095$).

APPENDIX B: QUASICLASSICAL SUPERPOSITION APPROXIMATION

Here we provide the expressions for the thermodynamic properties in the quasiclassical harmonic superposition approximation and in the quantum harmonic superposition approximation with anharmonic corrections. In these two ap-

Downloaded 25 May 2001 to 131.111.112.18. Redistribution subject to AIP license or copyright, see http://ojps.aip.org/jcpo/jcpcr.jsp

pendices, we consider an N-atom system at temperature $T=1/k_B\beta$, with $\kappa=3N-6$ the number of independent degrees of freedom. For a given set $\{\nu_\alpha^i\}$ of vibrational frequencies, $i=1,\ldots,\kappa$, $\overline{\nu}_\alpha$ is the geometric mean frequency, $\langle\nu_\alpha\rangle$ is the arithmetic mean frequency, and $\nu_\alpha^{\rm rms}$ is the root mean square frequency of minimum α.

The partition function of the single isomer α is given by Eq. (25), which includes the temperature-dependent quasiclassical Feynman–Hibbs effective potential,

$$Z_\alpha(\beta)=\frac{e^{-\beta E_\alpha^{\rm FH}(\beta)}}{(\beta h\overline{\nu}_\alpha)^\kappa}. \tag{B1}$$

Straightforward algebra leads to the following quasiclassical heat capacity, after summation of all individual contributions (B1),

$$C_v(\beta)=k_B\beta^2\left[\frac{Z_2-Z_c}{Z_0}+\frac{\kappa}{\beta^2}-\left(\frac{Z_1}{Z_0}\right)^2\right], \tag{B2}$$

with

$$Z_n(\beta)=\sum_\alpha n_\alpha(E_\alpha^{\rm FH})^n\frac{e^{-\beta E_\alpha^{\rm FH}}}{(\beta h\overline{\nu}_\alpha)^\kappa},\quad n=0,1,2, \tag{B3}$$

and

$$Z_c(\beta)=\frac{\kappa}{6}\sum_\alpha n_\alpha(h\nu_\alpha^{\rm rms})^2\frac{e^{-\beta E_\alpha^{\rm FH}}}{(\beta h\overline{\nu}_\alpha)^\kappa}. \tag{B4}$$

APPENDIX C: QUANTUM SUPERPOSITION WITH ANHARMONIC CORRECTIONS

By allowing all vibrational frequencies ν_α^i to be temperature-dependent, Eqs. (21)–(24) can be replaced by the following expression:

$$C_v(\beta)=k_B\beta^2\left[\frac{Z_2+2Z_{11}+Z_{02}-Z_c}{Z_0}-\left(\frac{Z_1+Z_{01}}{Z_0}\right)^2\right], \tag{C1}$$

where

$$Z_n=\sum_\alpha n_\alpha\left[E_\alpha+\sum_i\frac{h}{2}\frac{\partial\beta\nu_\alpha^i}{\partial\beta}\right]^n\frac{e^{-\beta E_\alpha^0}}{\Pi_i 1-e^{-\beta h\nu_\alpha^i}},\quad n=0,1,2, \tag{C2}$$

$$Z_{n1}=\sum_\alpha n_\alpha\left[E_\alpha+\sum_i\frac{h}{2}\frac{\partial\beta\nu_\alpha^i}{\partial\beta}\right]^n\frac{e^{-\beta E_\alpha^0}}{\Pi_i 1-e^{-\beta h\nu_\alpha^i}}\times\sum_j\frac{h\partial(\beta\nu_\alpha^j)/\partial\beta}{e^{\beta h\nu_\alpha^j}-1},\quad n=0,1, \tag{C3}$$

$$Z_{02}=\sum_\alpha\frac{n_\alpha e^{-\beta E_\alpha^0}}{\Pi_i 1-e^{-\beta h\nu_\alpha^i}}\left[\sum_j\frac{(h\partial(\beta\nu_\alpha^j)/\partial\beta)^2e^{-\beta h\nu_\alpha^j}}{(1-e^{-\beta h\nu_\alpha^j})^2}+\left(\sum_j\frac{h\partial(\beta\nu_\alpha^j)/\partial\beta}{e^{\beta h\nu_\alpha^j}-1}\right)^2\right], \tag{C4}$$

$$Z_c=\sum_\alpha\frac{n_\alpha e^{-\beta E_\alpha^0}}{\Pi_i 1-e^{-\beta h\nu_\alpha^i}}\sum_j\frac{h}{2}\left(\frac{\partial^2\beta\nu_\alpha^j}{\partial\beta^2}\right)\tanh\frac{\beta h\nu_\alpha^i}{2}. \tag{C5}$$

[1] M. P. Allen and D. J. Tildesley, *Computer Simulations of Liquids* (Oxford University Press, Oxford 1987).
[2] D. M. Ceperley, Rev. Mod. Phys. **67**, 279 (1995).
[3] C. Chakravarty, Int. Rev. Phys. **16**, 421 (1997).
[4] S. W. Rick, R. D. Leitner, J. D. Doll, D. L. Freeman, and D. D. Frantz, J. Chem. Phys. **95**, 6658 (1991); D. D. Frantz, D. L. Freeman, and J. D. Doll, *ibid.* **97**, 5713 (1992).
[5] J. P. Neirotti, D. L. Freeman, and J. D. Doll, J. Chem. Phys. **112**, 3990 (2000).
[6] C. Chakravarty, J. Chem. Phys. **102**, 956 (1995).
[7] C. Chakravarty, J. Chem. Phys. **103**, 10663 (1995).
[8] D. J. Chartrand and R. J. Le Roy, J. Chem. Phys. **108**, 8626 (1998).
[9] J. D. Doll, R. D. Coalson, and D. L. Freeman, Phys. Rev. Lett. **55**, 1 (1985).
[10] D. Thirumalai, R. W. Hall, and B. J. Berne, J. Chem. Phys. **81**, 2523 (1984).
[11] C. Chakravarty, M. C. Gordillo, and D. M. Ceperley, J. Chem. Phys. **109**, 2123 (1998).
[12] R. P. Feynman and A. R. Hibbs, *Quantum Mechanics and Path Integrals* (McGraw–Hill, New York, 1965).
[13] E. Wigner, Phys. Rev. **40**, 749 (1932); J. G. Kirkwood, *ibid.* **44**, 31 (1933).
[14] J.-P. Hansen and I. R. McDonald, *Theory of Simple Liquids* (Academic, New York, 1986).
[15] M. Neumann and M. Zoppi, Phys. Rev. A **40**, 4572 (1989).
[16] L. M. Sesé, Mol. Phys. **76**, 1335 (1992).
[17] S. Liu, G. K. Horton, and E. R. Cowley, Phys. Rev. B **44**, 11714 (1991).
[18] J. Cao and G. A. Voth, J. Chem. Phys. **102**, 3337 (1995); **103**, 4211 (1995).
[19] D. R. Reichman and G. A. Voth, J. Chem. Phys. **112**, 3267 (2000); **112**, 3280 (2000).
[20] F. H. Stillinger and T. A. Weber, Phys. Rev. A **25**, 978 (1982).
[21] D. J. Wales, Mol. Phys. **78**, 151 (1993).
[22] G. Franke, E. R. Hilf, and P. Borrmann, J. Chem. Phys. **98**, 3496 (1993).
[23] R. J. Speedy, J. Mol. Struct. **485+486**, 573 (1999); S. Sastry, J. Phys.: Condens. Matter **12**, 6523 (2000).
[24] J. P. K. Doye and D. J. Wales, Phys. Rev. Lett. **80**, 1357 (1998); J. P. K. Doye, M. A. Miiller, and D. J. Wales, J. Chem. Phys. **109**, 8143 (1999).
[25] J. P. K. Doye and D. J. Wales, J. Chem. Phys. **111**, 11070 (1999).
[26] F. H. Stillinger, J. Chem. Phys. **89**, 4180 (1988).
[27] J. A. Hodgdon and F. H. Stillinger, J. Chem. Phys. **102**, 457 (1995).
[28] C. Chakravarty, R. J. Hinde, D. L. Leitner, and D. J. Wales, Phys. Rev. E **56**, 363 (1997).
[29] C. Chakravarty and R. Ramaswamy, J. Chem. Phys. **106**, 5564 (1997); C. Chakravarty, Phys. Rev. B **59**, 3590 (1999).
[30] J. P. K. Doye, M. A. Miiller, and D. J. Wales, J. Chem. Phys. **111**, 8417 (1999).
[31] C. Chakravarty, J. Chem. Phys. **104**, 7223 (1996).
[32] D. Marx, S. Sengupta, and P. Nielaba, J. Chem. Phys. **99**, 6031 (1993).
[33] Y. Fujiwara, T. O. Osborn, and S. F. J. Wilk, Phys. Rev. A **25**, 14 (1982).
[34] C. J. Geyer, in *Computing Science and Statistics: Proceedings of the 23rd Symposium on the Interface* (American Statistical Association, New York, 1991).
[35] F. Calvo and F. Spiegelmann, J. Chem. Phys. **112**, 2888 (2000).
[36] M. Bixon and J. Jortner, J. Chem. Phys. **91**, 1631 (1989).
[37] R. S. Berry, J. Jellinek, and G. Natanson, Chem. Phys. Lett. **107**, 227 (1984).
[38] D. J. McGinty, J. Chem. Phys. **55**, 580 (1971); J. J. Burton, *ibid.* **56**, 3123 (1972).
[39] D. J. Wales and I. Ohmine, J. Chem. Phys. **98**, 7245 (1993).
[40] J. P. K. Doye and D. J. Wales, J. Chem. Phys. **102**, 9659 (1995).
[41] K. D. Ball and R. S. Berry, J. Chem. Phys. **109**, 8541 (1998).
[42] M. A. Miiller, J. P. K. Doye, and D. J. Wales, Phys. Rev. E **60**, 3701 (1999).
[43] A. P. Miiller and B. N. Brockhouse, Can. J. Phys. **49**, 704 (1991).
[44] P. Labastie and R. L. Whetten, Phys. Rev. Lett. **65**, 1567 (1990).
[45] A. L. Mackay, Acta Crystallogr. **15**, 916 (1962).
[46] F. Calvo and J. P. K. Doye, Phys. Rev. E **63**, 10902(R) (2001).
[47] J. P. K. Doye, D. J. Wales, and R. S. Berry, J. Chem. Phys. **103**, 4234 (1995).
[48] J. P. K. Doye, M. A. Miiller, and D. J. Wales, J. Chem. Phys. **110**, 6896 (1999).
[49] J. P. Neirotti, F. Calvo, D. L. Freeman, and J. D. Doll, J. Chem. Phys. **112**,

Downloaded 25 May 2001 to 131.111.112.18. Redistribution subject to AIP license or copyright, see http://ojps.aip.org/jcpo/jcpcr.jsp

10340 (2000); F. Calvo, J. P. Neirotti, D. L. Freeman, and J. D. Doll, *ibid.* **112**, 10350 (2000).
[50] F. Calvo and P. Labastie, Chem. Phys. Lett. **247**, 395 (1995).
[51] P. Sindzingre, D. M. Ceperley, and M. L. Klein, Phys. Rev. Lett. **67**, 1871 (1991); V. Buch, J. Chem. Phys. **100**, 7610 (1994).
[52] D. Scharf, G. J. Martyna, and M. L. Klein, J. Chem. Phys. **97**, 3590 (1992).
[53] Z. Li and H. A. Scheraga, Proc. Natl. Acad. Sci. U.S.A. **84**, 6611 (1987).
[54] D. J. Wales and J. P. K. Doye, J. Phys. Chem. A **101**, 5111 (1997).
[55] J. A. Northby, J. Chem. Phys. **87**, 6166 (1987).
[56] R. H. Leary and J. P. K. Doye, Phys. Rev. E **60**, R6320 (1999).
[57] D. J. Wales, J. P. K. Doye, A. Dullweber, F. Y. Naumkin, and F. Calvo, The Cambridge Cluster Database, URL ⟨http://www-wales.ch.cam.ac.uk/CCD.html⟩.
[58] T. D. Märk and P. Scheier, Chem. Phys. Lett. **137**, 245 (1987).
[59] I. A. Harris, R. S. Kidwell, and J. A. Northby, Phys. Rev. Lett. **53**, 2390 (1984).
[60] S. R. Elliott, *The Physics and Chemistry of Solids* (Wiley, New York, 1998).
[61] J. Jortner, Z. Phys. D: At., Mol. Clusters **24**, 247 (1992).
[62] M. Schmidt and H. Haberland (private communication).
[63] M. Schmidt, R. Kusche, B. von Issendorff, and H. Haberland, Nature (London) **393**, 238 (1998).
[64] J. Ma, D. Hsu, and J. E. Straub, J. Chem. Phys. **99**, 4024 (1993).

Downloaded 25 May 2001 to 131.111.112.18. Redistribution subject to AIP license or copyright, see http://ojps.aip.org/jcpo/jcpcr.jsp